Self-Sustainable Communications With RF Energy Harvesting: Ginibre Point Process Modeling and Analysis

Lu, Xiao; Flint, Ian; Niyato, Dusit; Privault, Nicolas; Wang, Ping

2016

Lu, X., Flint, I., Niyato, D., Privault, N., & Wang, P. (2016). Self-Sustainable Communications With RF Energy Harvesting: Ginibre Point Process Modeling and Analysis. IEEE Journal on Selected Areas in Communications, 34(5), 1518-1535.

https://hdl.handle.net/10356/84594

https://doi.org/10.1109/JSAC.2016.2551538

Self-Sustainable Communications with RF Energy Harvesting: Ginibre Point Process Modeling and Analysis

Xiao Lu, Ian Flint, Dusit Niyato, *Senior Member, IEEE*, Nicolas Privault, Ping Wang, *Senior Member, IEEE*

***Abstract*—RF-enabled wireless power transfer and energy harvesting has recently emerged as a promising technique to provision perpetual energy replenishment for low-power wireless networks. The network devices are replenished by the RF energy harvested from the transmission of ambient RF transmitters, which offers a practical and promising solution to enable self-sustainable communications. This paper adopts a stochastic geometry framework based on the Ginibre model to analyze the performance of self-sustainable communications over cellular networks with general fading channels. Specifically, we consider the point-to-point downlink transmission between an access point and a battery-free device in the cellular networks, where the ambient RF transmitters are randomly distributed following a repulsive point process, called Ginibre α-determinantal point process (DPP). Two practical RF energy harvesting receiver architectures, namely time-switching and power-splitting, are investigated. We perform an analytical study on the RF-powered device and derive the expectation of the RF energy harvesting rate, the energy outage probability and the transmission outage probability over Nakagami-m fading channels. These are expressed in terms of so-called Fredholm determinants, which we compute efficiently with modern techniques from numerical analysis. Our analytical results are corroborated by the numerical simulations, and the efficiency of our approximations is demonstrated. In practice, the accurate simulation of any of the Fredholm determinant appearing in the manuscript is a matter of seconds. An interesting finding is that a smaller value of α (corresponding to larger repulsion) yields a better transmission outage performance when the density of the ambient RF transmitters is small. However, it yields a lower transmission outage probability when the density of the ambient RF transmitters is large. We also show analytically that the power-splitting architecture outperforms the time-switching architecture in terms of transmission outage performances. Lastly, our analysis provides guidelines for setting the time-switching and power-splitting coefficients at their optimal values.**

Index terms- Wireless energy harvesting, self-sustainable communications, wireless powered communication networks, simultaneous wireless information and power transfer, Nakagami-m fading, Internet of things, time-switching, power-splitting, determinantal point process, Ginibre model.

Xiao Lu is with Department of Electrical and Computer Engineering, University of Alberta, Canada.

Ian Flint and Nicolas Privault are with School of Physical and Mathematical Sciences, Nanyang Technological University, Singapore.

Dusit Niyato and Ping Wang are with School of Computer Engineering, Nanyang Technological University, Singapore

Ian Flint is the corresponding author.

I. Introduction

Wireless communication powered by energy harvested from the natural environment, e.g., wind and tide, or power sources such as wireless energy transmitters has enabled self-sustainable communications maintaining and operating in an autonomous manner, without human intervention [1]. Self-sustainable communications, understood to integrate various technologies including signal processing, circuit design, power scavenging and management, etc., is envisioned to be the next momentous development in the green mobile ecosystem. The technologies will pave the way towards emerging paradigms such as Internet of things (IoTs) [2], machine-type communications (MTC) [3], and autonomous sensor networking [4].

Energy efficiency and perpetual maintenance are two critical issues in self-sustainable communications. Accordingly, simultaneous wireless information and power transfer (SWIPT) and RF energy harvesting techniques [5]–[7] have recently emerged as a practical and effective solution. On one hand, energy efficiency is significantly improved by recycling the ambient RF signals that are not captured by the intended receivers. On the other hand, extracting energy from RF signals that pervasively exists in wireless communication systems renders perpetual maintenance and even battery-free implementation for low-power energy-constrained electrical equipments [8], such as IoT sensors and radio frequency identification (RFID) tags. Moreover, as the wireless energy is carried by the same RF signals that delivers wireless information, RF energy harvesting becomes a particularly suitable alternative technique for replenishing wireless communication devices [9], [10].

Recently, SWIPT has drawn great research attention and been intensively investigated, e.g., in point-to-point channels [11], broadcast channels [12], relay channels [13], multi-antenna channels [14], [15], OFDMA channels [16], opportunistic channels [17] and wiretap channels [18]. Moreover, cooperative SWIPT in distributed systems have been investigated in [19]. There has also been a growing interest in exploring SWIPT with full-duplex techniques [20], [21]. For hardware implementation, as reviewed in [22], various prototype platforms have been demonstrated for ambient RF energy harvesting, e.g., from cellular networks and digital TV signals, which indicates the practicality of self-sustainable operation of real devices by optimizing their duty cycle. For example, a recent measurement in [23] reported that an RF-to-DC conversion efficiency of 40% and an output dc voltage of

224 mV can be achieved by a dual-band RF energy harvester for GSM-1800 and UMTS-2100 bands. The emerging self-sustainable communications with RF energy harvesting has found its applications in low-power wireless systems, such as RFID systems [24], [25], wireless renewable sensor networks [22], body area networks [26], [27], and backscatter communication systems [28]–[30]. RF-powered communications is also expected to have a profound impact on the development of IoT [31] and machine-to-machine communications [32]. The readers are referred to the recent survey in [33] for detailed overview of existing applications of RF-powered communications and envisioned future applications.

A. Related Work

Recently, there have been growing interests from academia, industry, and standardization bodies on investigating RF energy harvesting. The existing efforts have primarily focused on the hardware circuit design to improve the energy harvesting efficiency as well as the resource allocation and performance analysis in wireless networks with RF energy harvesting. An up-to-date survey on the advance of RF powered communication networks can be found in [34].

For statistical modeling of large-scale RF energy harvesting networks, stochastic geometry is a suitable tool that models random spatial patterns by a point process. Poisson point processes (PPPs) have been widely adopted to model the spatial configuration of various types of wireless networks with RF energy harvesting. The existing literature has primarily focused on cellular networks and relay networks. The authors in [35] characterized the tradeoffs among transmit power and density of mobile devices and wireless power beacons. The distributions of mobile devices and power beacons are modeled as two homogeneous PPPs. In [36], the authors investigated the transmission probability and the coverage probability of the uplink transmission in a multiple-tier cellular network. As for relay networks, the authors in [37] analyzed the outage performance and the average harvested energy for a large-scale network with transmitter-receiver pairs distributed as a PPP. A random relay selection scheme was analyzed for randomly located relay nodes distributed following an independent PPP. In [38], the authors derived the probability of successful data exchange and the network lifetime gain in a two-way network coding enabled relay network modeled by PPPs, where the relay node is powered by the RF information sources. The authors in [39] applied PPP modeling to analyze relay strategies in a randomly located network. The outage probability and diversity gain have been characterized for three different relay strategies to facilitate a comparison of their performance.

Moreover, the research efforts have also investigated RF energy harvesting in cognitive radio network [40] and device-to-device (D2D) networks [41]. Reference [40] considered the scenario wherein a secondary cognitive sensor network opportunistically harvests energy from the transmissions of the primary network. The authors optimized the maximum throughput of the secondary network under the constraints of an outage probability for both networks, which were modeled as two independent PPPs. The study in [41] investigated D2D communication powered by the RF energy from the overlying cellular networks. By modeling the cellular base stations, mobiles, and D2D devices as three independent PPPs, the authors derived the network performance in terms of the transmission probability and outage probabilities for both D2D transmitters and cellular mobiles. In addition, reference [42] studied a generic RF-powered network, where the wireless nodes and the access points are distributed as two independent PPPs. Given a successful information transmission probability constraint, the authors maximized the spatial throughput for wireless nodes in both battery-free and battery-deployment cases.

Though the PPP offers a simple modeling framework with analytical tractability, it fails to characterize the correlation among the locations of the network agents. The weakness of PPP modeling lies in the fact that the spatial points may be located too close to each other due to their independence [43]. In real-world network scenarios, the distribution of network components may exhibit repulsive behaviors. This repulsion is indeed a common phenomenon in wireless systems, e.g., sensor networks [44]. An instance in real network design is that RF transmitters such as cellular base stations, access points, relay nodes and data sinks, are not deployed too close to each other [45], [46], which is evidence of repulsive behavior.

Recently, the Ginibre point process (GPP) [47], which is a type of repulsive point process, has been advocated to model random phenomena where repulsion is observed, e.g., in [48] and [49]. Existing studies have applied the GPP [50], the α-GPP [51], and the β-GPP [48], [52] to model locations of base stations in conventional wireless networks. Our previous work in [49], [53] utilized a Ginibre determinantal point process to model the distribution of ambient RF transmitters in a wireless powered sensor network with deterministic propagation channels. However, the closed form expressions of the considered performance metrics are not available. Instead, we were able to provide the lower bounds of the performance metrics which were interpreted as the worst-case performance. In this work, we consider a cellular network with general fading channels and, using a conditioning technique inspired by the seminal work of [43], we analyze the general-case network performance and provide good approximations of the performance metrics.

B. Motivations and Contributions

For self-sustainable communications, interference from ambient RF transmitters impairs the capacity of communications. However, the interference is also instrumental for an RF-powered device, as it can be converted to useful energy. To understand the role of the interference, it is critical to analyze how the RF signals from randomly-located ambient RF transmitters, e.g., cellular mobiles, impact the overall performance of self-sustainable communications. Moreover, most of the existing literature only considers either SWIPT (e.g., in [11] and [12]) or ambient RF energy harvesting (e.g., in [41] and [49]). However, in real networks, it is not practical

to perform only SWIPT from a dedicated RF energy source without the consideration of ambient RF transmitters. This is because an RF energy harvester is designed to work on certain frequency band(s), e.g., 900MHz or 1800MHz. Any received RF signal within the range of the target frequency of the energy harvester will be converted into energy, as long as the input power density exceeds the sensitivity of the rectifier. Therefore, we aim to study a realistic network scenario, where a decided energy source performs SWIPT coexists with ambient RF energy transmitters to be energy sources of an RF-powered device. Additionally, the distribution of ambient RF transmitters may demonstrate various patterns in different environments. It is interesting to investigate how the distribution of the ambient transmitters influences the performance of an RF-powered device. To this end, we adopt a novel repulsive point process called Ginibre α-determinantal point process (DPP) to model the network distribution. The factor α is able to capture different degrees of repulsion among points, and also covers the Poisson point process (PPP) when $\alpha = 0$. These are the main motivations behind our study in this work.

In this paper, we investigate the performance of self-sustainable communications with RF energy harvesting over cellular networks. Specifically, we consider the point-to-point downlink transmission from a base station or an access point to a battery-free network device, which is powered by the energy harvested from randomly-located ambient RF transmitters. Our main contributions are summarized below.

- First, we derive the closed-form expectation of the aggregated energy harvesting rate of the RF-powered device as a function of the density of ambient transmitters. Numerical results corroborate our closed-form expressions.
- Next, we analyze the energy outage probability, i.e. the probability that the RF-powered device experiences a blackout due to insufficient energy. Our derivation provides semi-closed form expressions for the energy outage probability. By this we mean that the error committed in the approximation is well-controlled and can be quantified mathematically, cf. e.g. Theorem 2. It is confirmed by simulation that the expressions provide very accurate estimation of the energy outage probability. The analysis further shows that a larger repulsion among the ambient transmitters reduces the energy outage probability.
- Furthermore, we study the quality of service (QoS) metric, namely, the transmission outage probability, which is defined as the probability that the RF-powered device is unable to meet its information throughput requirement, due to an insufficient transmit power and/or interference. We again derive an expression for the transmission outage probability in semi-closed form, which matches the simulation results. Our analysis shows that there exists a tradeoff between the interference signal received by the information receiver and the RF energy harvested by the energy harvester. This tradeoff is significantly influenced by the density of ambient RF transmitters and the minimum throughput requirement.

Our mathematical contributions rely heavily on Lemma 1.

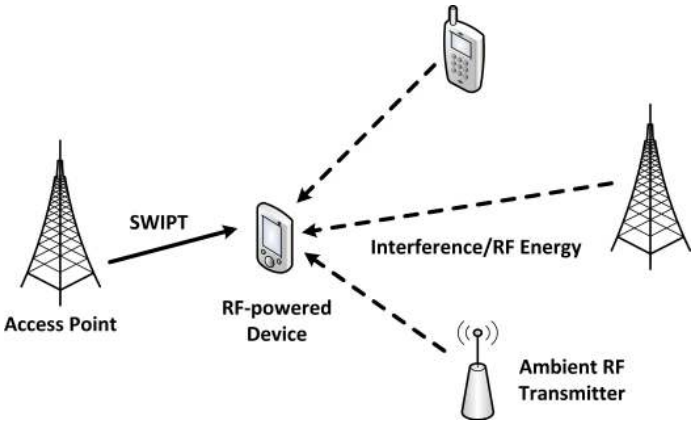

Fig. 1. A network model of downlink transmission for an RF-powered device over a cellular network.

This powerful lemma allows us to give precise approximations of the performance metrics in terms of Fredholm determinants, which will be defined later in Section II-B1. To the best of our knowledge, the computation of performance metrics by means of Fredholm determinants is a novel technique, and is shown to be an efficient way to compute the relevant quantities. The algorithms used in this paper for the numerical computation of Fredholm determinants of general operators improve the state of the art. We obtain fast and reliable estimations of the Fredholm determinants involved in our main results, compared with the alternative of computing the performance metrics by Monte Carlo estimation.

The remainder of this paper is organized as follows. Section II describes the system model, the stochastic geometry model, and the performance metrics. Section III estimates the performance metrics of the RF-powered device over a cellular network with randomly-located ambient RF transmitters modeled as a Ginibre α-DPP. Section IV demonstrates the performance evaluation results. Finally, Section V concludes our work.

Notations: Throughout the paper, we use $\mathbb{E}[X]$ to denote the probabilistic expectation of a random variable X, $\mathbb{P}(A)$ to denote the probability of an event A. Moreover, we use $||\mathbf{x}||$ to represent the Euclidean distance between the coordinate $\mathbf{x}$ and the central point of the plane.

II. System Model

A. Network Model

We consider an RF-powered device powered solely by the energy harvested from the RF signals transmitted by ambient RF transmitters. We assume that the ambient RF transmitters are distributed as a general class of point processes, which will be specified in detail in Section II-B.

It is further assumed that the RF-powered device is battery-less. In other words, the device utilizes the instantaneously harvested RF energy to supply its operations. We investigate two co-located receiver architectures, namely, time-switching and power-splitting [34], as shown in Fig 1. These two co-located receiver architectures allow an energy harvester and

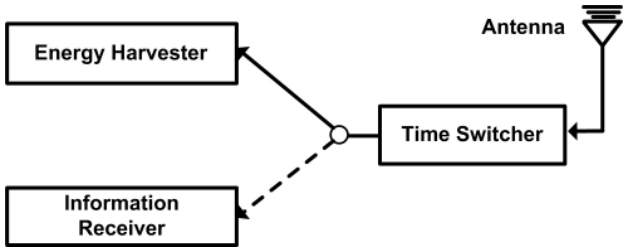

(a) Time Switching Achitecture

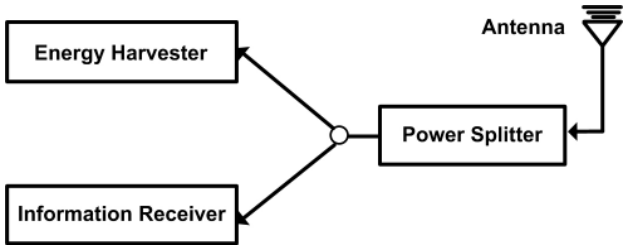

(b) Power Splitting Achitecture

an information decoder to share the same antenna, and both of them observe the same channel condition.

- Time-Switching Architecture: The time-switching architecture, shown in Fig. 2a, operates on a time-slot based manner. That is, either the information receiver or the RF energy harvester is connected to the antenna at a given time. Specifically, this architecture first uses τ portion of time to harvest energy. Then during the remaining $1-\tau$ portion of time, the RF-powered device uses the energy reserved from the capacitor to decode information.
- Power-Splitting Architecture: In the power-splitting architecture, shown in Fig. 2b, the received RF signals are divided into two streams with different power levels for the information decoder and RF energy harvester. The power splitter is able to adjust the power ratio between two streams. We denote the portion of RF signals flowed to the energy harvester by ρ, and that to the information receiver by $1-\rho$.

In this work, we consider downlink SWIPT from the base station or access point to the RF-powered device. For the time-switching architecture, the device alternately performs energy harvesting and information decoding. For the power-splitting architecture, the device performs energy harvesting and information decoding simultaneously. We assume that the capacitors of the both architectures are lossless.

1) Time-switching Architecture: The RF energy harvesting rate (in watts) by the device from the RF transmitter k in a fading channel P_{H}^{k} is given by [54]:

$$P_{\mathrm{H}}^{k}=\frac{\tau\beta P_{\mathrm{S}}h_k}{(d_k)^{\gamma}}, \tag{1}$$

where β is the RF-to-DC power conversion efficiency of the device, P_{S} is the transmit power of the RF transmitter k, $\gamma>0$ is the path-loss exponent, and h_k represents the channel power gain from the RF transmitter k to the device. For RF propagation, we consider a general channel power gain model following the gamma distribution with shape parameter δ and rate parameter θ. In other words, h_k are assumed to be i.i.d. random variables verifying

$$h_k\sim\Gamma(\delta,\theta),\quad \delta,\theta>0.$$

Note that $\delta=1$ recovers the case $h_k\sim\mathrm{Exp}(\theta)$. Lastly, d_k is the distance between the transmit antenna of an RF transmitter k to the receiver antenna of the RF-powered device. Let $\mathbf{x}_k\in\mathbb{R}^2$ be the coordinates of the RF transmitter k in a referential centered at the RF-powered device. In our model, $d_k=\epsilon+\|\mathbf{x}_k\|$, where ϵ is a fixed (small) parameter which ensures that the associated harvested RF power is finite in expectation. Physically, ϵ is the closest distance that the RF transmitters can be to the device.

Then, the aggregated RF energy harvesting rate by the device equipped with time-switching architecture is modeled as follows:

$$P_{\mathrm{H}}^{TS}=\frac{\overline{F}}{1+F}\sum_{k\in\mathcal{K}}P_{\mathrm{H}}^{k}=\frac{\overline{F}\tau\beta}{1+F}\left(\sum_{k\in\mathcal{K}}\frac{P_{\mathrm{S}}h_k}{(d_k)^{\gamma}}+\frac{P_{\mathrm{A}}h_A}{d_A^{\gamma_A}}\right), \tag{2}$$

where $\mathcal{K}$ is a random set consisting of all RF transmitters, P_A is the transmit power of the access point, d_A represents the distance between the transmit antenna of the access point and the receive antenna of the RF-powered device, h_{A} denotes the channel gain between the transmit antenna of the access point and the receive antenna of the RF-powered device, and it is assumed that $h_{\mathrm{A}}\sim\mathrm{Exp}(\lambda_{\mathrm{A}})$ for $\lambda_{\mathrm{A}}>0$. Here, F is a random variable independent of $\mathcal{K}$ and h_k, $k\in\mathcal{K}$. It is further assumed that $F\sim\mathrm{Exp}(\mu)$ for some constant $\mu>0$. The coefficient $\overline{F}$ is chosen so that this random noise has an expectation of 1. Namely, we set $\overline{F}:=\left(-\mu\,\mathrm{e}^{\mu}\,\mathrm{Ei}(-\mu)\right)^{-1}$ so that by the change of variable $u\equiv\mu(x+1)$,

$$\begin{aligned}\mathbb{E}\left[\frac{\overline{F}}{1+F}\right]&=\overline{F}\int_0^{\infty}\frac{\mu}{1+x}\,\mathrm{e}^{-\mu x}\,\mathrm{d}x\\&=\overline{F}\mu\,\mathrm{e}^{\mu}\int_{\mu}^{\infty}\frac{1}{u}\,\mathrm{e}^{-u}\,\mathrm{d}u=1,\end{aligned} \tag{3}$$

where here Ei is the exponential integral special function defined by

$$\mathrm{Ei}(x):=-\int_{-x}^{\infty}\frac{1}{u}\,\mathrm{e}^{-u}\,\mathrm{d}u,\quad x\neq 0.$$

Let us note that the coefficient $\overline{F}/(1+F)$ is unusual; it can be understood as a random noise (e.g. electrical or in the channel) in the detection of the actual harvested energy. We assume that $\mathcal{K}$ is a point process [55] independent of the h_k.

The maximum transmission rate of the access point is evaluated according to the following model[1]:

$$C^{TS}=\begin{cases}(1-\tau)W\log_2\left(1+\frac{h_{\mathrm{A}}P_{\mathrm{A}}/\|\mathbf{x}_{\mathrm{A}}\|^{\gamma_{\mathrm{A}}}}{\sigma^2+\xi I^{TS}}\right) & \text{if } P_{\mathrm{H}}^{TS}\geq P_{\mathrm{C}},\\ 0 & \text{if } P_{\mathrm{H}}^{TS}<P_{\mathrm{C}},\end{cases} \tag{4}$$

where W is the transmission bandwidth, σ^2 is a nonnegative constant which represents the power of additive white Gaussian noise (AWGN). By analogy, $\mathbf{x}_{\mathrm{A}}$ represents the coordinates

[1]Note that state-of-the-art wireless information receivers are not yet able to achieve this rate upper bound due to additional processing noise such as the RF band to baseband conversion noise.

of the access point in the referential centered at the RF-powered device, P_{A} denotes the transmit power of the access point, and $\gamma_{\mathrm{A}} > 0$ is the path-loss exponent between the transmit antenna of the access point and the receive antenna of the RF-powered device. The device consumes a base circuit power, denoted by P_{C}. Following practical models [56], the circuit power consumption of the device is assumed to be fixed. Here, I^{TS} denotes the interference from ambient RF transmitters at the transmission link of the access point, for the case of time-switching, and can be evaluated as follows:

$$I^{TS} = \sum_{k\in\mathcal{K}} \frac{P_{\mathrm{S}} h_k}{(d_k)^{\gamma}}. \tag{5}$$

Lastly, $\xi \in [0,1]$ is an interference coefficient, which represents the fraction of the total interference RF transmitters that impacts the transmission rate. Specifically $\xi = 0$ corresponds the case without interference and $\xi = 1$ is the worst case wherein it is assumed that all RF sources contribute fully to the interference at the access point.

2) Power-splitting Architecture: Analogously, the aggregated RF energy harvesting rate by the RF-powered device equipped in the power-splitting architecture in a unit time is modeled as

$$P_{\mathrm{H}}^{PS} = \frac{\bar{F}\rho\beta}{1+F}\left(\sum_{k\in\mathcal{K}} \frac{P_{\mathrm{S}} h_k}{(d_k)^{\gamma}} + \frac{P_{\mathrm{A}} h_A}{d_A^{\gamma}}\right). \tag{6}$$

In the power-splitting architecture, the downlink information rate can be computed as [54]:

$$C^{PS} = \begin{cases} W\log_2\left(1+\frac{(1-\rho)h_{\mathrm{A}}P_{\mathrm{A}}/\|\mathbf{x}_{\mathrm{A}}\|^{\gamma_{\mathrm{A}}}}{\sigma_{SP}^2+(1-\rho)\sigma^2+\xi I^{PS}}\right) & \text{if } P_{\mathrm{H}}^{PS} \geq P_{\mathrm{C}}, \\ 0 & \text{if } P_{\mathrm{H}}^{PS} < P_{\mathrm{C}}, \end{cases} \tag{7}$$

where σ_{SP} is the signal processing noise power. Here, I^{PS} denotes the interference from the ambient RF transmitter after power splitting, which is modeled as

$$I^{PS} = (1-\rho)\sum_{k\in\mathcal{K}} \frac{P_{\mathrm{S}} h_k}{(d_k)^{\gamma}}. \tag{8}$$

The main notations used in this paper are summarized in Table I.

B. Geometric DPP Modeling of Ambient RF Transmitters

As an extension of the Poisson setting, we model the locations of RF transmitters using a point process $\mathcal{K}$ on an observation window $O \subset \mathbb{R}^2$ such that $0 < |O| < +\infty$. here $|O|$ denotes the Lebesgue measure of O. In other terms, $\mathcal{K}$ is an almost surely finite random collection of points inside O. We refer to [55] and [57] for the general theory of point processes. In the aforementioned references are defined the correlation functions $\zeta^{(n)}$ of $\mathcal{K}$ *w.r.t.* the Lebesgue measure on $\mathbb{R}^2$, and which verify

$$\mathbb{E}\left[\prod_{i=1}^{n}\mathcal{K}(B_i)\right] = \int_{B_1\times\cdots\times B_n} \zeta^{(n)}(x_1,\ldots,x_n)\,\mathrm{d}x_1\cdots\mathrm{d}x_n, \tag{9}$$

for any family of mutually disjoint bounded subsets $B_1,\ldots,B_n$ of $\mathbb{R}^2$, $n \geq 1$. Heuristically, $\zeta^{(1)}$ is the spatial particle density, and $\zeta^{(n)}(x_1,\ldots,x_n)\,\mathrm{d}x_1\cdots\mathrm{d}x_n$ is the probability of finding a point of the point process in the vicinity of each x_i, $i = 1,\ldots,n$. The correlation functions are thus a generalization of the concept of the probability density function to the framework of point processes. The correlation functions play an important role in the definition and interpretation of a general α-DPP.

1) General α-determinantal point process: We let $\alpha = -1/j$ for an integer $j > 0$, and we define a general α-DPP in the following. Let us introduce a map $K : \mathrm{L}^2(\mathbb{R}^2) \mapsto \mathrm{L}^2(\mathbb{R}^2)$, where $\mathrm{L}^2(\mathbb{R}^2)$ is the space of square integrable functions on $\mathbb{R}^2$. We assume in the following that $\mathcal{K}$ satisfies Condition A from [58], recalled below.

Hypothesis 1. *Assume that the map $\mathcal{K}$ is a Hilbert-Schmidt operator from $\mathrm{L}^2(\mathbb{R}^2)$ into $\mathrm{L}^2(\mathbb{R}^2)$ which satisfies the following conditions:*

1) *K is a bounded symmetric integral operator on $\mathrm{L}^2(\mathbb{R}^2)$, with kernel still denoted by $K(\cdot,\cdot)$;*
2) *The spectrum of K is included in $[0, -1/\alpha]$;*
3) *The map K is locally of trace-class (see [59] for a proper definition).*

The map K is called the *kernel* of the α-DPP. It represents the interaction force between the different points of the point process. A locally finite and simple point process on $\mathbb{R}^2$ is called an α-DPP if its correlation functions *w.r.t.* the Lebesgue measure on $\mathbb{R}^2$ (defined in (9)) exist and satisfy

$$\zeta^{(n)}(\mathbf{x}_1,\ldots,\mathbf{x}_n) = \det_{\alpha}(K(\mathbf{x}_i,\mathbf{x}_j))_{1\leq i,j\leq n}, \tag{10}$$

for any $n \geq 1$ and $\mathbf{x}_1,\ldots,\mathbf{x}_n \in \mathbb{R}^2$, where the α-determinant of a matrix $M = (M_{ij})_{1\leq i,j\leq n}$ is defined as

$$\det_{\alpha} M = \sum_{z\in S_n} \alpha^{n-\nu(z)} \prod_{i=1}^{n} M_{iz(i)}, \tag{11}$$

where S_n stands for the n-th symmetric group and $\nu(z)$ is the number of cycles in the permutation $z \in S_n$. We note that (11) generalizes the usual definition of the determinant (obtained for $\alpha = -1$) and was initially introduced in [60].

Let us now give some basic properties of the α-DPP to emphasize the role played by the kernel K. We start by a proposition exhibiting the repulsion properties of the α-DPP. Its proof follows from the definition of the correlation functions (9).

Proposition 1 (Repulsion of the α-DPP)**.** *The covariance of an α-DPP of kernel K is given by*

$$\mathrm{Cov}(\mathcal{K}(A),\mathcal{K}(B)) = \alpha\int_{A\times B} |K(\mathbf{x},\mathbf{y})|^2\,\mathrm{d}\mathbf{x}\mathrm{d}\mathbf{y},$$

where $\mathcal{K}(A)$ and $\mathcal{K}(B)$ denote the random number of point process points located within the disjoint bounded sets $A \subset \mathbb{R}^2$ and $B \subset \mathbb{R}^2$, respectively.

Since $\alpha < 0$, $\mathcal{K}(A)$ and $\mathcal{K}(B)$ are negatively correlated and the associated α-DPP is known to be locally Gibbsian, see, e.g., [61], therefore it is a type of repulsive point process. As $\alpha \to 0$, $\mathcal{K}(A)$ and $\mathcal{K}(B)$ tend not to be correlated, and in fact it can be shown that the corresponding point process converges weakly to the PPP, cf. [58].

TABLE I
NOTATIONS.

Symbol	Definition
α	Repulsion factor
β	RF-to-DC power conversion efficiency of the RF-powered device
d_k	The distance between the transmit antenna of RF transmitter k and the receiver antenna of the RF-powered device
γ	Pass-loss exponent
h_A	The channel gain between the access point and RF-powered device
h_k	The channel gain between the ambient RF transmitter k and RF-powered device
κ	Minimum information throughput requirement
P_{C}	The circuit power consumption of the RF-powered device
P_{A}	The transmit power of the access point
P_{S}^k	The transmit power of RF transmitter $k \in \mathcal{K}$
P_H^{TS}, P_H^{PS}	The RF energy harvesting rate of the time-switching and power-splitting architecture, respectively
ρ	The portion of RF signals harvested by a power-splitting architecture
σ^2	The power density of AWGN
σ_{SP}^2	The power density of signal processing noise
τ	The portion of time a time-switching receiver working on energy harvesting mode
$\mathbf{x}_i$	The coordinates of the RF-powered device
$\mathbf{x}_k$	The coordinates of the RF transmitter k
W	The bandwidth of the channel between the access point and RF-powered device
ξ	Interference coefficient
ζ	The spatial density of ambient RF transmitters

Next, we recall from [62] the following proposition which gives the hole probabilities of the α-DPP. Proposition 2 allows us to compute the quantities known as hole probabilities.

Proposition 2 (Hole probability of the α-DPP)**.** *For every bounded set $B \subset \mathbb{R}^2$ we have*

$$\mathbb{P}(\mathcal{K} \cap B = \emptyset) = \mathrm{Det}(\mathrm{Id} + \alpha K_B)^{-1/\alpha}, \tag{12}$$

where $K_B(\mathbf{x},\mathbf{y}) \triangleq 1_B(\mathbf{x})K(\mathbf{x},\mathbf{y})1_B(\mathbf{y})$, and 1_B denotes the indicator function of a set B. Here, Id is the identity operator on $\mathrm{L}^2(B)$ and for any trace class integral operator K, $\mathrm{Det}\,(\mathrm{Id} + \alpha K)$ is the Fredholm determinant of $\mathrm{Id} + \alpha K$ which is defined as

$$\mathrm{Det}(\mathrm{Id} - \alpha K)^{-1/\alpha} = \sum_{n \geq 0} \frac{1}{n!} \int \det_\alpha(K(x_i, x_j))_{1 \leq i,j \leq n} \, \mathrm{d}x_1 \cdots \mathrm{d}x_n, \tag{13}$$

as long as $|\alpha| \leq 1$. (13) was obtained in Theorem 2.4 of [58], see also [59] for more details on the Fredholm determinant.

Lastly, we recall from [58] the following proposition which gives the Laplace transform of the α-DPP.

Proposition 3 (Laplace transform of the α-DPP)**.** *For any $\varphi : \mathbb{R}^2 \to [0, +\infty)$,*

$$\mathbb{E}\left[\exp\left(-\sum_{k \in \mathcal{K}} \varphi(\mathbf{x}_k)\right)\right] = \mathrm{Det}(\mathrm{Id} + \alpha K_\varphi)^{-1/\alpha}, \tag{14}$$

where K_φ is the Hilbert-Schmidt operator with kernel

$$\sqrt{1 - \mathrm{e}^{-\varphi(\mathbf{x})}} K(\mathbf{x},\mathbf{y}) \sqrt{1 - \mathrm{e}^{-\varphi(\mathbf{y})}}, \quad \mathbf{x},\mathbf{y} \in \mathbb{R}^2.$$

2) The Ginibre point process: In the rest of the paper, we focus on the Ginibre α-DPP, which is a particular α-DPP well-suited for applications. The Ginibre process is a type of α-DPP that is invariant with respect to rotations. Therefore, it is fruitful for computational convenience to restrict our attention to the choice of observation window $O = \mathcal{B}(0, R)$, defined as a disc centered around 0 and of radius $R > 0$.

The Ginibre process is defined by the so-called Ginibre kernel given by

$$K(\mathbf{x},\mathbf{y}) = \zeta \, e^{\pi\zeta \mathbf{x}\bar{\mathbf{y}}} e^{-\frac{\pi\zeta}{2}(|\mathbf{x}|^2 + |\mathbf{y}|^2)}, \quad \mathbf{x},\mathbf{y} \in O = \mathcal{B}(0, R), \tag{15}$$

where $\zeta > 0$ is a fixed parameter called *spatial density* of the point process. This kernel is that of the usual Ginibre process defined, e.g., in [47], to which we have applied a homothety of parameter $\sqrt{\pi\zeta} > 0$: $x \mapsto x/(\sqrt{\pi\zeta})$. The associated α-DPP exists since the kernel (15) satisfies Condition A from [58]. We begin by recalling a few key features of the Ginibre process.

- The intensity function of the Ginibre process is given by
$$\zeta^{(1)}(\mathbf{x}) = K(\mathbf{x},\mathbf{x}) = \zeta, \tag{16}$$
cf. [58]. This means that the average number of points in a bounded set $B \subset \mathcal{B}(0, R)$ is $\zeta\,|B|$. Note that the intensity function of a homogeneous PPP is also a constant, so ζ is interpreted as the intensity of the corresponding PPP.
- The Ginibre α-DPP is stationary and isotropic in the sense that its distribution is invariant with respect to translations and rotations, cf. [47]. Hence, the Ginibre point process models a situation where the RF transmitters are distributed homogeneously in the plane.

We note that the constant intensity (16) and the invariance with respect to rotations might in some cases not be practical. However, these hypotheses may be lifted. Namely, the kernel (15) may be modified in order to account for an inhomogeneous spatial density, and all the main results of this paper may be written in terms of the eigenvalues of the modified kernel.

Next, we mention that the Ginibre α-DPP used here is different from the so-called β-Ginibre process introduced in [63] and used as a model for wireless networks in [48]. The Ginibre α-DPP ($-1 \leq \alpha < 0$) is a superposition of $-1/\alpha$ independent copies of a Ginibre DPP with an intensity

multiplied by $\sqrt{-\alpha}$, while the β-Ginibre ($0 < \beta < 1$) is obtained by deleting the points of a Ginibre DPP independently and with probability $1-\beta$ and by applying a homothety of ratio $\sqrt{\beta}$ to the remaining points (cf. [63]). Both classes offer a (different) parametrization of a range of point processes between the Ginibre process and the PPP. We also note that our calculations can be extended to the class of β-Ginibre processes with no major technical difficulties. Different variations of the Ginibre point process have been successfully applied to model phenomena from wireless communication, cf. [48], [50]–[52] among others. We choose here the α-GPP instead of its alternatives since its construction by superposition of independent repulsive processes yields a natural physical interpretation of the repulsion as happening on distinct independent layers, e.g. on 2 different frequency bands for the $(-1/2)$-DPP. Additionally, we remark there is no additional complexity involved in this choice and most results will be expressed in terms of the Fredholm either way.

We write $\mathcal{K} \sim \mathrm{Gin}(\alpha, \zeta)$ when $\mathcal{K}$ is an α-DPP with the Ginibre kernel defined in (15) and spatial density ζ. Since K is a Hermitian compact operator, the spectral theorem for Hermitian and compact operators yields the decomposition $K(\mathbf{x},\mathbf{y}) = \sum_{n\geq 0} \lambda_n \varphi_n(\mathbf{x})\overline{\varphi_n(\mathbf{y})}$, where $(\varphi_i)_{i\geq 0}$ is a basis of eigenvectors of $\mathrm{L}^2(O)$, and $(\lambda_i)_{i\geq 0}$ are the corresponding eigenvalues. In, e.g., [47], it is shown that the eigenvalues of the Ginibre point process on $O = \mathcal{B}(0,R)$ are given by

$$\lambda_n = \frac{\Gamma(n+1, \pi\zeta R^2)}{n!}, \qquad n \in \mathbb{N}, \tag{17}$$

where

$$\Gamma(z,a) \triangleq \int_0^a \mathrm{e}^{-t} t^{z-1}\,\mathrm{d}t, \qquad z \in \mathbb{C}, \quad a \geq 0, \tag{18}$$

is the lower incomplete Gamma function. Furthermore, the eigenvectors of K are given by $\varphi_n(z) \triangleq \frac{1}{\sqrt{\lambda_n}} \frac{\sqrt{\zeta}}{\sqrt{n!}} \mathrm{e}^{-\frac{\pi\zeta}{2}|z|^2} (\sqrt{\pi\zeta} z)^n$, for $n \in \mathbb{N}$ and $z \in O$. We refer to [47] for further mathematical details on the Ginibre point process.

Remark. *Combining the contents of Section II-B1 and Section II-B2, we summarize the main characteristics of the Ginibre α-DPP, where $\alpha \in [-1, 0]$.*

- *The intensity function of the Ginibre α-DPP is ζ, cf. (16). In other words the average number of points in a bounded set $B \subset \mathcal{B}(0,R)$ is $\zeta\,|B|$.*
- *The Ginibre α-DPP is stationary and isotropic.*
- *Letting $A, B \subset \mathbb{R}^2$ be two disjoint bounded sets, we have*

$$\mathrm{Cov}(\mathcal{K}(A), \mathcal{K}(B)) = \alpha\zeta \int_{A\times B} e^{-\pi\zeta\|\mathbf{x}-\mathbf{y}\|^2}\,\mathrm{d}\mathbf{x}\mathrm{d}\mathbf{y} \leq 0,$$

by Proposition 1, which contrasts with the PPP wherein the above covariance is zero.

C. Performance Metrics

We define the performance metrics of the RF-powered device as the expectation of RF energy harvesting rate, average energy outage probability, and average transmission outage probability. The mathematical quantities of interest are then defined in the following.

The expectation of the RF energy harvesting rate is defined as $E_{P_\mathrm{H}} \triangleq \mathbb{E}[P_\mathrm{H}]$. Energy outage occurs when the RF-powered device cannot harvest sufficient RF energy from the ambiance to operate the circuit. The energy outage probability is defined as $P_{eo} \triangleq \mathbb{P}(P_\mathrm{H} < P_\mathrm{C})$. Moreover, we are interested in the QoS metric defined as a transmission outage probability. Let $\kappa \geq 0$ denote the minimum information throughput requirement. If the RF-powered device fails to obtain enough throughput, it incurs a transmission outage. Note that the transmission outage occurs in two cases, namely when there is an energy outage, and when the decoded information throughput is less than the minimum requirement under the condition that there is enough harvested power. Therefore, the transmission outage probability can be calculated as

$$P_{to} \triangleq \mathbb{P}(P_\mathrm{H} < P_\mathrm{C}) + \mathbb{P}(C < \kappa, P_\mathrm{H} \geq P_\mathrm{C}). \tag{19}$$

The computation of the key performance metrics involve the so-called Fredholm determinant introduced in Proposition 2. The numerical computation of the Fredholm determinant is a largely unexplored area, see the excellent survey [64]. The Fredholm determinants appearing in this paper (cf. for example Theorem 2 and Theorem 3) involve 2-dimensional Hilbert-Schimidt operators, whereby an adapted version of the main (1-dimensional) algorithm of [64] is required. It should be noted that the numerical evaluation of Fredholm determinants is orders of magnitude faster than the alternative Monte-Carlo techniques, cf. the rate of convergence obtained in Theorem 6.2. of [64]. This heuristic is observed in the algorithm that we used; the Monte-Carlo simulations were much more time-consuming.

III. Analytical formulas

In this section we estimate the metrics defined in Section II-C when $\mathcal{K} \sim \mathrm{Gin}(\alpha, \zeta)$ is the Ginibre α-DPP with parameter $\alpha = -1/j$ (for some positive integer j), and density $\zeta > 0$.

The performance metrics defined in the previous section might be estimated by Monte Carlo simulation of the underlying α-DPP. Simulation of α-DPPs when $\alpha < 0$ is done by using the Schmidt orthogonalization algorithm developed in full generality in [65], and specifically in [47] for the Ginibre point process. The simple generalization of the algorithm to $\alpha < 0$ can be found in the survey [66], and additional details on DPP can be found in [67].

The results from this section are primarily based on the following lemma which is a generalization of the ideas from [43] to the context of α-determinantal point processes.

Lemma 1. *Let $\mathcal{K} \sim \mathrm{Gin}(\alpha, \zeta)$ and $(h_k)_{k\in\mathbb{N}}$ a sequence of mutually independent and identically distributed random variables, independent of $\mathcal{K}$, and with moment generating function denoted by*

$$M_h(t) := \mathbb{E}\left[\mathrm{e}^{th_1}\right], \quad t \leq 0,$$

defined on the nonpositive reals. Then for any nonnegative $\varphi : \mathbb{R}^2 \to [0, +\infty)$,

$$\mathbb{E}\left[\exp\left(-\sum_{k\in\mathcal{K}} h_k \varphi(\mathbf{x}_k)\right)\right] = \mathrm{Det}\left(\mathrm{Id} + \alpha A\right)^{-1/\alpha},$$

where Det *denotes the Fredholm determinant, A is the integral operator with kernel,*

$$A(\mathbf{x},\mathbf{y}) = \sqrt{1-M_h(-\varphi(\mathbf{x}))}K(\mathbf{x},\mathbf{y})\sqrt{1-M_h(-\varphi(\mathbf{y}))}, \quad \mathbf{x},\mathbf{y}\in\mathbb{R}^2, \tag{20}$$

and K is defined in (15).

For brevity, the proof of **Lemma 1** is presented in **Appendix I**.

The Monte Carlo methods used to compute the quantities in Section II-C can be time-consuming in practice, especially when Monte Carlo estimation is repeatedly applied to multiple values of the parameters. Thus, in many applications, it is of major interest to have some (semi-)closed forms for the performance metrics, which we now present. We will study in more detail the time-switching architecture as well as the power-splitting architecture in the following subsections.

A. Time-Switching Architecture

We start with the time-switching architecture. The expectation of RF energy harvesting rate is evaluated in the following theorem, which is similar to Theorem 1 in [49]. Although there is a slight overlap with our results in [49], we write here all the details since the context is different and we proceed in a different manner.

Theorem 1. *The expectation of RF energy harvesting rate in the time-switching architecture is explicitly computed as follows:*

$$\mathbb{E}\left[P_{\mathrm{H}}^{TS}\right] = \tau\beta\left(\frac{P_{\mathrm{A}}}{\theta_{\mathrm{A}}\|x_{\mathrm{A}}\|^{\gamma_{\mathrm{A}}}} + \frac{2\pi\zeta P_{\mathrm{S}}\delta}{\theta}\int_0^R \frac{r}{(r+\epsilon)^{\gamma}}\,\mathrm{d}r\right). \tag{21}$$

Furthermore, the integral appearing in (21) has a closed form given by

$$\int_0^R \frac{r}{(r+\epsilon)^{\gamma}}\,\mathrm{d}r = \begin{cases} \frac{\left(\epsilon^{2-\gamma}-(R+\epsilon)^{1-\gamma}(\epsilon+(\gamma-1)R)\right)}{(\gamma-2)(\gamma-1)} & \text{if } \gamma\neq 1 \text{ and } \gamma\neq 2,\\ R-\epsilon\ln\left(1+R/\epsilon\right) & \text{if } \gamma=1,\\ \ln\left(1+R/\epsilon\right)-\frac{R}{R+\epsilon} & \text{if } \gamma=2. \end{cases} \tag{22}$$

The proof of **Theorem 1** is shown in **Appendix II**.

We now give an expression of approximation energy outage probability in the case of the time-switching architecture. Note that the computation of the energy outage probability is equivalent to that of the probability density function of RF energy harvesting rate, computed at P_{C}. Recall that in Theorem 2, P_{H}^{TS} is given by (2).

Theorem 2. *The energy outage probability is in the following interval:*

$$\mathbb{P}\left(P_{\mathrm{H}}^{TS} < P_{\mathrm{C}}\right) \in \left[\left(1+\frac{\mu\tau\beta P_{\mathrm{A}}\overline{F}}{\theta_{\mathrm{A}}P_{\mathrm{C}}\|\mathbf{x}_{\mathrm{A}}\|^{\gamma_{\mathrm{A}}}}\right)^{-1}\mathrm{Det}\left(\mathrm{Id}+\alpha A\right)^{-1/\alpha}, \left(1+\frac{\mu\tau\beta P_{\mathrm{A}}\overline{F}}{\theta_{\mathrm{A}}P_{\mathrm{C}}\|\mathbf{x}_{\mathrm{A}}\|^{\gamma_{\mathrm{A}}}}\right)^{-1}\mathrm{Det}\left(\mathrm{Id}+\alpha A\right)^{-1/\alpha} + \left(1-\mathrm{e}^{-\mu}\right)\right], \tag{23}$$

where Det *denotes the Fredholm determinant, A is the integral operator with kernel*

$$A(\mathbf{x},\mathbf{y}) = \sqrt{1-\left(1+\frac{\mu\tau\beta P_{\mathrm{S}}\overline{F}}{\theta P_{\mathrm{C}}(\|\mathbf{x}\|+\epsilon)^{\gamma}}\right)^{-\delta}} \times K(\mathbf{x},\mathbf{y})\sqrt{1-\left(1+\frac{\mu\tau\beta P_{\mathrm{S}}\overline{F}}{\theta P_{\mathrm{C}}(\|\mathbf{y}\|+\epsilon)^{\gamma}}\right)^{-\delta}}, \quad \mathbf{x},\mathbf{y}\in\mathbb{R}^2, \tag{24}$$

and where K is the kernel of the Ginibre determinantal point process defined in (15).

We note that Theorem 2 implies the approximation

$$\mathbb{P}\left(P_{\mathrm{H}}^{TS} < P_{\mathrm{C}}\right) \simeq \left(1+\frac{\mu\tau\beta P_{\mathrm{A}}\overline{F}}{\theta_{\mathrm{A}}P_{\mathrm{C}}\|\mathbf{x}_{\mathrm{A}}\|^{\gamma_{\mathrm{A}}}}\right)^{-1} \times \mathrm{Det}\left(\mathrm{Id}+\alpha A\right)^{-1/\alpha},$$

and the error is less than or equal to $1-\mathrm{e}^{-\mu}$ which in turn is bounded by μ.

The readers are refered to **Appendix III** for the proof of **Theorem 2**.

Furthermore, we derive the transmission outage probability in the setting of the time-switching architecture based on (4).

Theorem 3. *The transmission outage probability of the time-switching architecture may be approximated by (25), where A_m and B_m is given by (26) and (27), respectively, and K is defined in (15).*

Although the result of Theorem 3 is an approximation of the transmission outage probability, it will be shown in Section IV that the approximation is in practice very close to the actual value. For brevity, the proof of **Theorem 3** is shown in **Appendix IV**.

B. Power-splitting Architecture

We now study the power-splitting architecture. From a mathematical point of view, these two architectures merely differ by a shift of the constants. Thus, the proofs in this section will be corollaries of those of Section III-A and we skip some details.

As in Section III-A, we begin by computing the expectation of the RF energy harvesting rate, based on (6).

$$\mathbb{P}\left(C^{TS}<\kappa\right)$$
$$\simeq 1-\exp\left(-\frac{\theta_{\mathrm{A}}\sigma^2\|\mathbf{x}_{\mathrm{A}}\|^{\gamma_{\mathrm{A}}}}{P_{\mathrm{A}}}\left(2^{\kappa/(W(1-\tau))}-1\right)\right)\left(\mathrm{Det}\left(\mathrm{Id}+\alpha A_m\right)^{-1/\alpha}-\left(1+\frac{\mu\tau\beta P_{\mathrm{A}}\overline{F}}{P_{\mathrm{C}}\|\mathbf{x}_{\mathrm{A}}\|^{\gamma_{\mathrm{A}}}\theta_{\mathrm{A}}}\right)^{-1}\mathrm{Det}\left(\mathrm{Id}+\alpha B_m\right)^{-1/\alpha}\right), \tag{25}$$

$$A_m(\mathbf{x},\mathbf{y})=\sqrt{1-\left(1+\frac{\theta_{\mathrm{A}}\|\mathbf{x}_{\mathrm{A}}\|^{\gamma_{\mathrm{A}}}P_{\mathrm{S}}\xi\left(2^{\kappa/(W(1-\tau))}-1\right)}{\theta P_{\mathrm{A}}(\|\mathbf{x}\|+\epsilon)^{\gamma}}\right)^{-\delta}}K(\mathbf{x},\mathbf{y})\sqrt{1-\left(1+\frac{\theta_{\mathrm{A}}\|\mathbf{x}_{\mathrm{A}}\|^{\gamma_{\mathrm{A}}}P_{\mathrm{S}}\xi\left(2^{\kappa/(W(1-\tau))}-1\right)}{\theta P_{\mathrm{A}}(\|\mathbf{y}\|+\epsilon)^{\gamma}}\right)^{-\delta}}, \tag{26}$$

$$\begin{aligned}B_m(\mathbf{x},\mathbf{y})=&\sqrt{1-\left(1+\frac{\theta_{\mathrm{A}}\|\mathbf{x}_{\mathrm{A}}\|^{\gamma_{\mathrm{A}}}P_{\mathrm{S}}P_{\mathrm{C}}\xi\left(2^{\kappa/(W(1-\tau))}-1\right)+\mu\tau\beta P_{\mathrm{S}}P_{\mathrm{A}}\overline{F}}{\theta P_{\mathrm{A}}P_{\mathrm{C}}\|(\mathbf{x}\|+\epsilon)^{\gamma}}\right)^{-\delta}}\\&\times K(\mathbf{x},\mathbf{y})\sqrt{1-\left(1+\frac{\theta_{\mathrm{A}}\|\mathbf{x}_{\mathrm{A}}\|^{\gamma_{\mathrm{A}}}P_{\mathrm{S}}P_{\mathrm{C}}\xi\left(2^{\kappa/(W(1-\tau))}-1\right)+\mu\tau\beta P_{\mathrm{S}}P_{\mathrm{A}}\overline{F}}{\theta P_{\mathrm{A}}P_{\mathrm{C}}(\|\mathbf{y}\|+\epsilon)^{\gamma}}\right)^{-\delta}},\end{aligned} \tag{27}$$

Theorem 4. *The expectation of RF energy harvesting rate in the power-splitting architecture is explicitly computed as*

$$\mathbb{E}\left[P_{\mathrm{H}}^{PS}\right]=\rho\beta\left(\frac{P_{\mathrm{A}}}{\theta_{\mathrm{A}}\|x_{\mathrm{A}}\|^{\gamma_{\mathrm{A}}}}+\frac{2\pi\rho P_{\mathrm{S}}\delta}{\theta}\int_0^R\frac{r}{(r+\epsilon)^{\gamma}}\,\mathrm{d}r\right), \tag{28}$$

where the integral appearing in (28) has a closed form given by (22).

Proof of Theorem 4. We simply note that the expression of P_{H}^{PS} given in (6) is simply P_{H}^{TS} with τ replaced by ρ. Hence Theorem 1 directly yields the result. □

Next, we give an expression of the energy outage probability in the case of a power-splitting architecture.

Theorem 5. *The energy outage probability is in the following interval:*

$$\begin{aligned}&\mathbb{P}\left(P_{\mathrm{H}}^{PS}<P_{\mathrm{C}}\right)\in\\&\left[\left(1+\frac{\mu\rho\beta P_{\mathrm{A}}\overline{F}}{\theta_{\mathrm{A}}P_{\mathrm{C}}\|\mathbf{x}_{\mathrm{A}}\|^{\gamma_{\mathrm{A}}}}\right)^{-1}\mathrm{Det}\left(\mathrm{Id}+\alpha A\right)^{-1/\alpha},\right.\\&\left.\left(1+\frac{\mu\rho\beta P_{\mathrm{A}}\overline{F}}{\theta_{\mathrm{A}}P_{\mathrm{C}}\|\mathbf{x}_{\mathrm{A}}\|^{\gamma_{\mathrm{A}}}}\right)^{-1}\mathrm{Det}\left(\mathrm{Id}+\alpha A\right)^{-1/\alpha}+\left(1-\mathrm{e}^{-\mu}\right)\right],\end{aligned} \tag{29}$$

where Det *denotes the Fredholm determinant, A is the integral operator with kernel*

$$\begin{aligned}A(\mathbf{x},\mathbf{y})=&\sqrt{1-\left(1+\frac{\mu\rho\beta P_{\mathrm{S}}\overline{F}}{\theta P_{\mathrm{C}}(\|\mathbf{x}\|+\epsilon)^{\gamma}}\right)^{-\delta}}\\&\times K(\mathbf{x},\mathbf{y})\sqrt{1-\left(1+\frac{\mu\rho\beta P_{\mathrm{S}}\overline{F}}{\theta P_{\mathrm{C}}(\|\mathbf{y}\|+\epsilon)^{\gamma}}\right)^{-\delta}},\\&\mathbf{x},\mathbf{y}\in\mathbb{R}^2,\end{aligned} \tag{30}$$

and K is defined in (15).

Proof of Theorem 5. We note that by the same arguments as in the proof of Theorem 4, Theorem 2 yields the result. □

Then, based on (7), we compute the transmission outage probability in the power-splitting architecture.

Theorem 6. *The transmission outage probability in the setting of the power-splitting architecture is given by (31), where A_m is the integral operator with kernel*

$$\begin{aligned}A_m(\mathbf{x},\mathbf{y})=&\sqrt{1-\left(1+\frac{\theta_{\mathrm{A}}\|\mathbf{x}_{\mathrm{A}}\|^{\gamma_{\mathrm{A}}}P_{\mathrm{S}}\left(2^{\kappa/W}-1\right)}{\theta P_{\mathrm{A}}(\|\mathbf{x}\|+\epsilon)^{\gamma}}\right)^{-\delta}}\\&\times K(\mathbf{x},\mathbf{y})\sqrt{1-\left(1+\frac{\theta_{\mathrm{A}}\|\mathbf{x}_{\mathrm{A}}\|^{\gamma_{\mathrm{A}}}P_{\mathrm{S}}\left(2^{\kappa/W}-1\right)}{\theta P_{\mathrm{A}}(\|\mathbf{y}\|+\epsilon)^{\gamma}}\right)^{-\delta}},\\&\mathbf{x},\mathbf{y}\in\mathbb{R}^2,\end{aligned} \tag{32}$$

and B_m is given by (33), and K is defined in (15).

Proof of Theorem 6. It suffices to notice that the expression of the maximum transmission rate C^{PS} given in (7) is precisely C^{TS} with $W(1-\tau)$ replaced with W, P_{A} replaced with $(1-\rho)P_{\mathrm{A}}$, and σ^2 replaced with $\sigma^2+(1-\rho)\sigma_{SP}^2$. Theorem 3 thus applies whilst applying the mentioned replacements. □

IV. Performance Analysis

In this section, we examine the validity and perform the analysis of the expressions derived in the previous section through numerical simulations. The network simulations in this paper are considered in the scenario of an LTE-A network, where an eNB performs downlink SWIPT to an MTC device enabled with RF energy harvesting capability. The overlaid network structure of MTC over cellular network has provided

$$\mathbb{P}(C^{PS}<\kappa) \simeq 1-\exp\left(-\frac{\theta_{\mathrm{A}}\left(\sigma^2+\sigma_{SP}^2/(1-\rho)\right)\|\mathbf{x}_{\mathrm{A}}\|^{\gamma_{\mathrm{A}}}}{P_{\mathrm{A}}}\left(2^{\kappa/W}-1\right)\right) \times\left(\mathrm{Det}\left(\mathrm{Id}+\alpha A_m\right)^{-1/\alpha}-\left(1+\frac{\mu\rho\beta P_{\mathrm{A}}\overline{F}}{P_{\mathrm{C}}\|\mathbf{x}_{\mathrm{A}}\|^{\gamma_{\mathrm{A}}}\theta_{\mathrm{A}}}\right)^{-1}\mathrm{Det}\left(\mathrm{Id}+\alpha B_m\right)^{-1/\alpha}\right), \tag{31}$$

$$B_m(\mathbf{x},\mathbf{y}) = \sqrt{1-\left(1+\frac{\theta_{\mathrm{A}}\|\mathbf{x}_{\mathrm{A}}\|^{\gamma_{\mathrm{A}}}P_{\mathrm{S}}P_{\mathrm{C}}\,\xi\left(2^{\kappa/W}-1\right)+\mu\rho\beta P_{\mathrm{S}}P_{\mathrm{A}}\overline{F}}{\theta P_{\mathrm{A}}P_{\mathrm{C}}(\|\mathbf{x}\|+\epsilon)^{\gamma}}\right)^{-\delta}} \times K(\mathbf{x},\mathbf{y})\sqrt{1-\left(1+\frac{\theta_{\mathrm{A}}\|\mathbf{x}_{\mathrm{A}}\|^{\gamma_{\mathrm{A}}}P_{\mathrm{S}}P_{\mathrm{C}}\,\xi\left(2^{\kappa/W}-1\right)+\mu\rho\beta P_{\mathrm{S}}P_{\mathrm{A}}\overline{F}}{\theta P_{\mathrm{A}}P_{\mathrm{C}}(\|\mathbf{y}\|+\epsilon)^{\gamma}}\right)^{-\delta}}, \quad \mathbf{x},\mathbf{y}\in\mathbb{R}^2, \tag{33}$$

a nature framework to facilitate RF energy harvesting for MTC devices from ambient cellular transmissions.

The eNB transmits on 46dBm (i.e., 39.81W) over a 20MHz channel following the specification 3GPP TS 36.942. The transmit power of ambient RF transmitters is set to be $100mW$ which is within the normal transmit power of cellular mobiles. The energy harvesting zone R is assumed to be 30m. The RF-to-DC power conversion efficiency is set to be 30%. The circuit power consumption of the MTC device is set to be 2.64μW as a recent circuit design in [68]. The incoming noise at the information receiver for both receiver architecture is assumed to be white Gaussian with power spectral density -120dBm/Hz [69], correspondingly 20nW over the 20MHz channel bandwidth. While the signal processing noise induced by the power splitter is assumed to be $10^{-6}\mu$W as in [70]. The other parameters take the values as shown in Table II unless otherwise stated.

TABLE II
PARAMETER SETTING.

Symbol	$\|\mathbf{x}_{\mathrm{A}}\|$	τ	ϱ	ϵ	μ	γ	m
Value	80m	0.5	0.5	0.05	0.01	4	0.05Mbps

We evaluate the performance of the MTC devices over Nakagami-m fading channels, which can be adjusted to fit different fading environments. Indeed, h_k ∼Nakagami(m, Ω), $m \geq 0.5$ is the shape parameter of the Nakagami distribution, which controls the Nakagami-m fading degree. Here, Ω= $2\sigma_I^2$ is the parameter which determines the spread of the Nakagami-m power density function, where $\sigma_I^2 = 1$ is the variance of the in-phase and in-quadrature components of the received signal envelope [71]. Our adopted channel model covers Nakagami(m, Ω) by setting $h_k \sim \Gamma(m, \frac{m}{\Omega})$ [72]. (Here, second parameter of the Gamma distribution is the rate.) Note that the Rayleigh distribution can be obtained with $m = 1$. Also, the results for the PPP can be obtained by choosing $\alpha = 0$ in the α-DPP setting. In addition, it can be observed from **Theorems 1**, **2**, **4** and **5** that the performance of the power-splitting architecture in terms of the expectation of the RF energy harvesting rate and average energy outage probability is identical to that of the time-switching architecture by substituting ρ to τ.

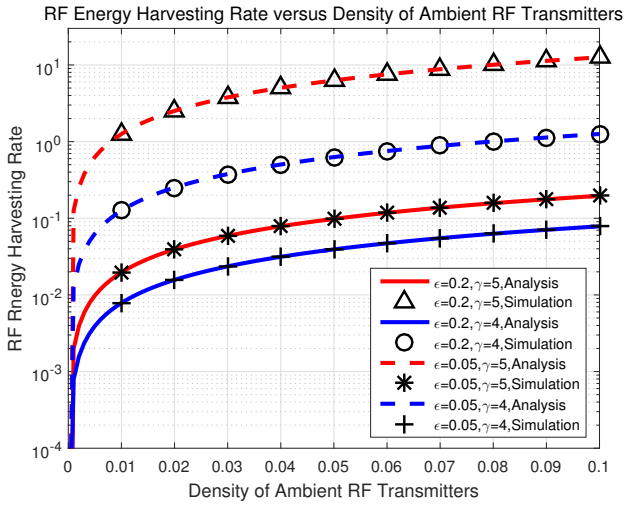

Fig. 2. Expectation of RF Energy Harvesting Rate versus Density of Ambient RF Transmitters.

We first examine the validity of the expectation of RF energy harvesting rate. Fig. 2 shows the results for $\gamma = 5$ and $\gamma = 4$ in Rayleigh fading channels (i.e., m=1). It can be seen that the numerical results, averaged over 10^7 of simulations, match accurately with the analytical expression given in (1) over a wide range of densities ζ, i.e., from 0 to 0.1. This is equivalent to the average number of ambient RF transmitters varying between 0 and 283. The RF energy harvesting rate is significantly affected by not only the path loss exponent γ but also ϵ. As expected, a larger (average) RF energy harvesting rate can be achieved when ϵ is small. The reason is straightforward as smaller ϵ indicates the ambient transmitters may stay closer to the RF-powered device, thus resulting in more energy harvesting rate. In addition, the degree of repulsion does not affect the average energy harvesting rate.

In Fig. 3, we illustrate the variation of the energy outage probability P_{eo} as a function of the density of ambient RF

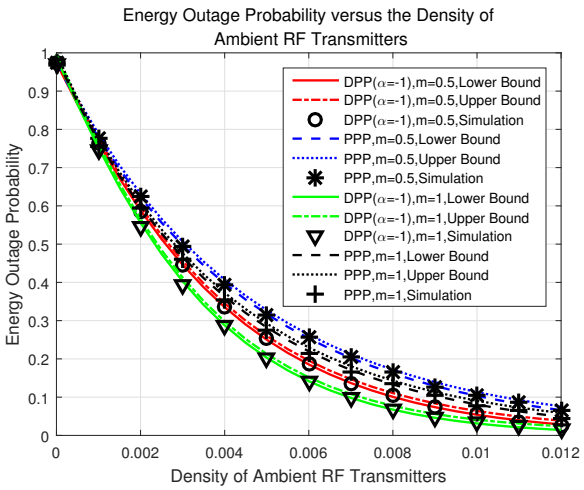

Fig. 3. Energy Outage Probability versus Density of Ambient RF Transmitters.

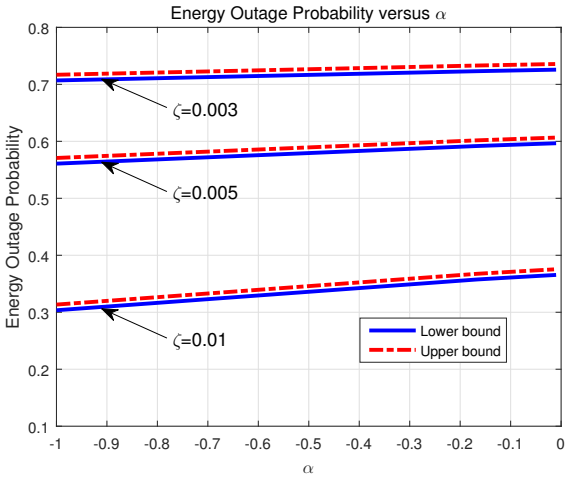

Fig. 4. Energy Outage Probability versus α (Rayleigh Fading).

transmitters ζ. The numerical results validate that the analytical expressions for the energy outage probability in (23) is accurate for different values of α under different fading factor m. Additionally, the error is expected to be less than $\mu = 0.01$ which is verified by simulation. We can see that P_{eo} is a monotonically decreasing function of ζ. In other words, the higher the density of ambient RF transmitters, the lower the chance the MTC device experiences an energy outage. Moreover, in an environment with smaller m, due to a larger RF energy harvesting rate, the MTC device experiences a smaller energy outage probability. Figure 4 further examines an impact of α on P_{eo}. A smaller value of α results in a lower energy outage probability. In other words, the more repulsion leads to the more scattering of the RF transmitters. Consequently, the chance that some RF transmitters are close to the MTC device to contribute enough energy is high, and a lower energy outage probability can be observed. Moreover, we observe that generally when the density ζ is larger, the variation of α results in a greater difference in the value of P_{eo}. The reason is that when the number of RF transmitters increases, strong attraction may generate more variance in the distribution pattern causing larger performance differences.

In Fig. 5, we evaluate how the value of time-switching coefficient τ influences the energy outage probability P_{eo} in the cases where the density ζ is 0.005 and 0.01. It can be seen that P_{eo} is a monotonically decreasing function of τ irrespectively of ζ. That is, the energy outage probability is minimized when τ takes the value of 1. From Fig. 5, we observe that when the density is large (e.g., ζ =0.01), the energy outage probability varies more dynamically with a change of τ than when the density is low (e.g.,, $\zeta = 0.005$).

Figure 6 demonstrates the impact of the circuit power consumption P_{C} of the MTC device on P_{eo} when the density ζ takes the value of 0.005 and 0.01. It is seen that P_{eo} is a monotonically increasing function of P_{C}. When the density is low (e.g., $\zeta = 0.005$), the corresponding performance shows a logarithm-like function. This shows that P_{eo} is more sensitive when P_{C} is small and becomes less sensitive when P_{C} is large. This implies that advances in circuit implementation to lower down P_{C} can render a considerable decrease of the energy outage probability, especially in the environment where the available ambient RF transmitters are scarce. Moreover, we observe that when ζ =0.005, the energy outage probability with the DPP (α =-1) approaches that with the PPP. Nevertheless, when ζ =0.01, the performance gap between the cases of the DPP (α =-1) and the PPP is wider. Therefore, the degree of repulsion α has more impact on P_{eo} when the density is low.

Next, we examine the analytical expressions for the transmission outage probability P_{to} in (25) and (31) for time-switching and power splitting architectures, respectively. Figure 7 illustrates the plots of P_{to} as a function of the density ζ for different values of α for both time-switching and power-splitting architectures. We observe that when the density ζ is low, i.e., smaller than 0.01, there exists some small gap between the simulation and analytical results. However, our derived approximation matches the simulation results better when ζ becomes larger. It can be found that P_{to} is a convex-like function of ζ. With the increase of the density ζ from 0, P_{to} first decreases then bounces up. The reason is that when ζ is small, the transmission outage is caused mostly by insufficient harvested energy. The increase of ζ will bring about more harvested energy, and thus decrease P_{to}. When ζ is larger than a certain value, the cause of the transmission outage becomes the excessive interference. Though the increase of ζ lowers the occurrence of an energy outage, the resulted incremental interference decreases the decoded information throughput, thus increasing P_{to}. Moreover, an interesting observation is that, a smaller α (larger repulsion) will not always be beneficial to achieve a lower P_{to}. This is different from the impact of α on P_{eo} wherein a smaller α always induces a lower P_{eo}. In particular, when the density is low, e.g., $\zeta = 0.005$, a smaller α results in a lower P_{to}. However, when the density is high, e.g., $\zeta = 0.03$, a larger α (stronger attraction) is helpful to reduce P_{to}. The reason can also be understood from the perspective of the distribution of RF transmitters. When the density ζ is small, transmission outage is caused primarily by insufficient harvested energy. Recall that a smaller α induces a lower P_{eo}, which also helps to generate a smaller P_{to}. However, when the density ζ is large, the occurrence of a transmission outage is caused

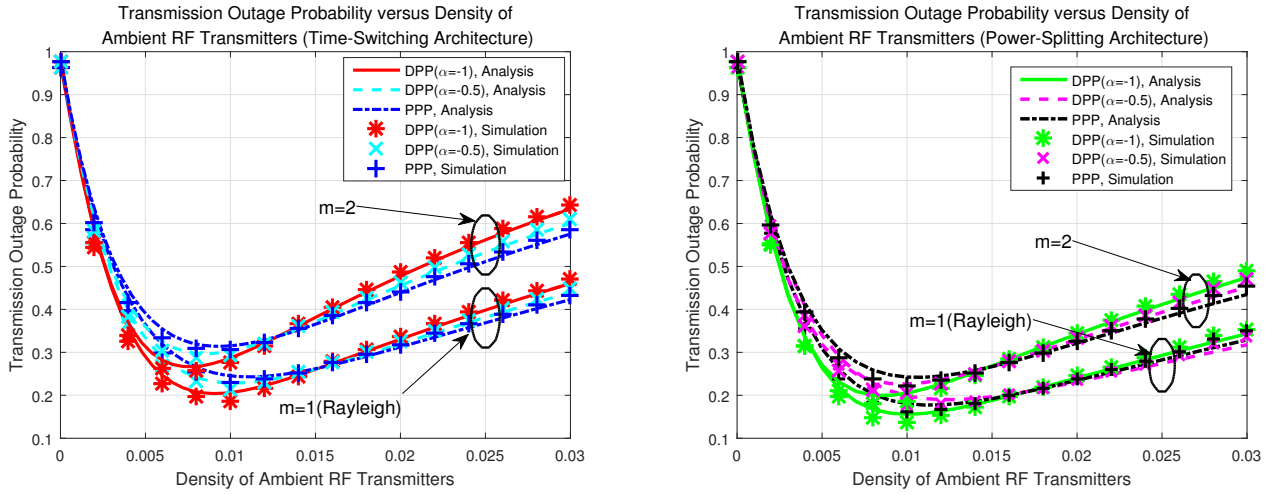

(a) Time-Switching Achitecture

(b) Power-Splitting Achitecture

Fig. 7. Transmission Outage Probability versus Density of Ambient RF Transmitters.

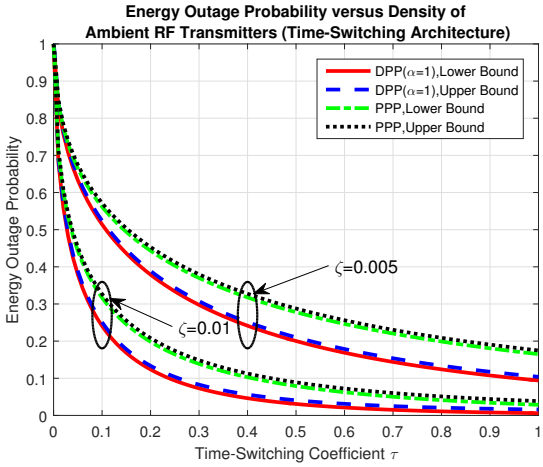

Fig. 5. Energy Outage Probability versus Time-Switching Coefficient τ (Rayleigh Fading).

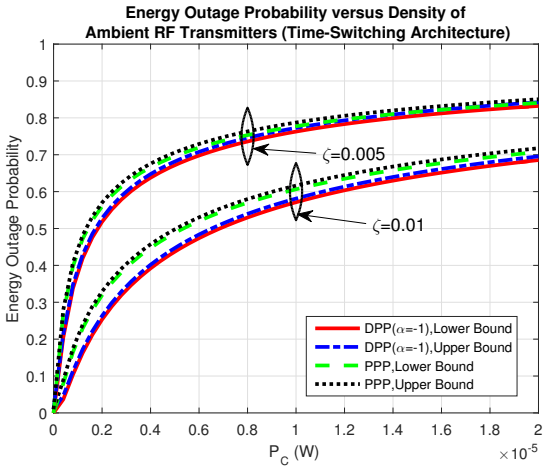

Fig. 6. Energy Outage Probability versus Circuit Power Consumption (Rayleigh Fading).

mainly by impaired throughput due to enlarged interference. Therefore, the DPP (corresponding to α =-1) yields better performance than that of the PPP when ζ is low and provides worse performance when ζ is high.

In Fig. 8, we study the influence of the time-switching coefficient τ on P_{eo} under different densities ζ. (As the power-splitting coefficient ρ results in a similar impact on P_{to}, we omit presenting the corresponding plots.) It is shown that P_{to} is also a convex-like function of τ. Specifically, when τ varies from 0 to 1, P_{to} first decreases from 100% and then increases back to 100% after reaching its minimum point. This is because there exists an optimal tradeoff in harvesting energy and receiving information. Either a smaller τ that gives less energy or a larger τ that diminishes the information throughput which causes an increase in P_{to}. Furthermore, it is obvious that the optimal value of τ is dependent on the density ζ. The larger ζ is, the smaller the optimal τ. The reason is straightforward as a smaller proportion of time is required to harvest sufficient energy in an environment with larger density ζ. Furthermore, when the throughput requirement is high, τ should decrease to let a larger portion of the time be used for receiving information.

We then compare the time-switching and power-splitting architectures directly in terms of the transmission outage probability. Fig. 9 shows P_{to} as a function of an energy harvesting ratio (τ for time-switching and ϱ for power-splitting) under different minimum throughput requirements and densities ζ. We observe that the power-splitting architecture always outperforms the time-switching architecture. In particular, with the adjustment of the energy harvesting ratio from 0 to 1, the performance gap between the two architectures first increases and then declines. The power-splitting architecture has a significant performance advantage over the time-switching architecture, especially when ρ is around its optimal value to minimize P_{to}. The reason can be intuitively understood as follows. P_{to} is determined by both the energy harvesting rate and the information decoding time. When the energy

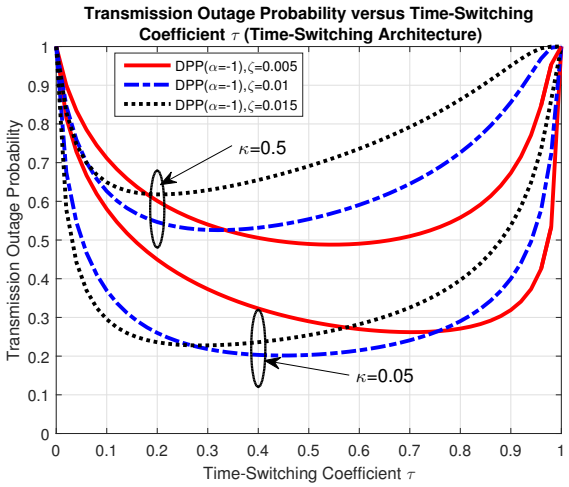

Fig. 8. Transmission Outage Probability versus Time-Switching Coefficient τ (Rayleigh Fading).

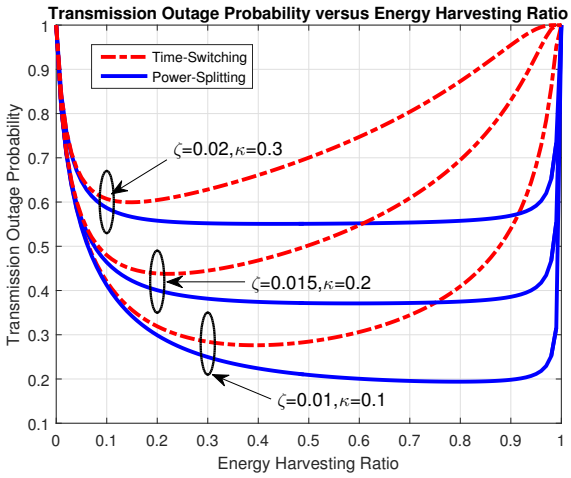

Fig. 9. Transmission Outage Probability versus Energy Harvesting Ratio (Rayleigh Fading) .

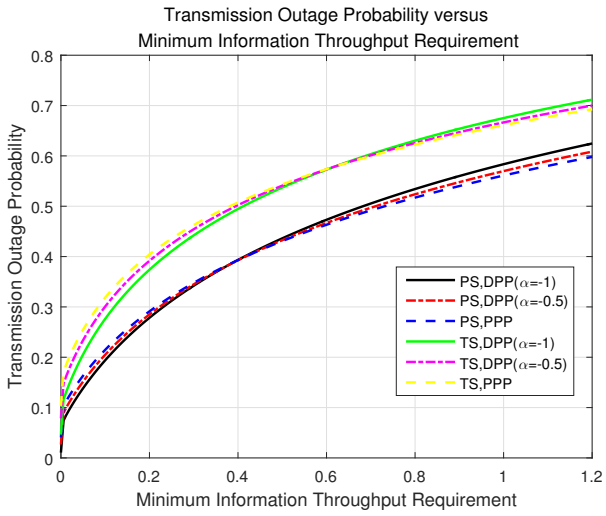

Fig. 10. Transmission Outage Probability versus Minimum Information Throughput Requirement (Rayleigh fading).

harvesting ratio is small, transmission outage is mainly caused by insufficient harvested energy. As the expressions of P_{eo} for both time-switching and power-splitting have the same function for their corresponding energy harvesting ratio, the performance difference for P_{to} of both architectures is small when the energy harvesting ratio is small. However, when the energy harvesting ratio is large (i.e., with a larger energy harvesting ratio), P_{to} is mainly affected by the information decoding time. The information decoding time of the time-switching architecture is only (1-τ) times that of the power-splitting architecture. Therefore, the latter outperforms the former when the energy harvesting ratio is large.

From Fig. 9, the optimal energy harvesting ratio obtained to minimize P_{to} is $\tau = 0.4$ and $\rho = 0.81$, when $\kappa = 0.1$. Under this optimal setting of energy harvesting ratio, we then demonstrates in Fig. 10 how P_{to} varies with the minimum information throughput requirement κ. The time-switching and power-splitting architectures are labeled as TS and PS, respectively. We can see that the plots are a log-like function, which indicates that κ has larger impact on P_{to} when κ takes small values. Another observation is that for both architectures, larger repulsion (e.g., $\alpha = -1$) results in lower P_{to} when κ is small, however, induces higher P_{to} when κ becomes large. This is because when the κ is small, P_{to} is mainly caused by insufficient harvested energy. As we have observed from above, larger repulsion renders higher energy harvesting rate thus results in smaller P_{to}. While when the κ is large, interference becomes the dominate factor on P_{to}. In this case, larger attraction (e.g., PPP) induces less interference thus actually brings about better perform.

Next, we investigate the mutual impact of the density ζ and the interference coefficient ξ as well as the transmit power P_{A} and P_{S} on the transmission outage probability. Fig. 11 demonstrates the role of the interference coefficient ξ on the transmission outage probability P_{to}. It can be observed that ξ tends to have a larger impact on P_{to} in an environment with a larger ζ. When the density of ambient RF transmitters is high (e.g., ζ =0.05), P_{to} is very sensitive to the variation of ξ, especially when ξ varies in a small range (e.g., from 0 to 0.4). An implication is that in a large-area network, a channel experiencing less interference should be assigned to MTC devices with a higher density of ambient transmitters. On the contrary, channels suffer high interference can be allocated to MTC devices with a lower density of ambient transmitters, as P_{to} becomes less sensitive in that context.

In Fig. 12, we show how the transmit power of the eNB and the ambient RF transmitter affect P_{to}, when ζ=0.01. As expected, increasing P_{A} monotonically decreases P_{to}. It is also found that P_{to} is a concave-like function of P_{S}. This reveals a tradeoff between the energy harvesting rate and the interference caused by the ambient transmitters. In a small range, e.g., P_{S} <0.03, the increase of P_{S} markedly improves the energy harvesting rate to lower down P_{to}. However, when P_{S} is greater than a certain threshold, the increase of P_{S} causes additional interference to impair the throughput, thus amplifying P_{to}.

For future work, the access point can adopt MIMO [73]. In this case, the transmission performance can be derived based

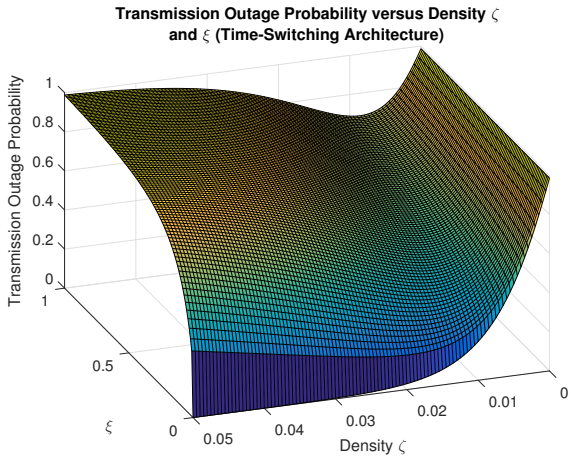

Fig. 11. Transmission Outage Probability versus density ζ and interference coefficient ξ ($\zeta = 0.01$, Rayleigh Fading).

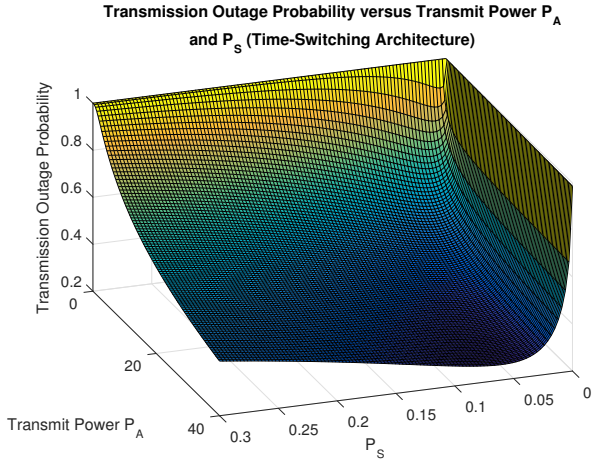

Fig. 12. Transmission Outage Probability versus transmit power P_{A} and P_{S} ($\zeta = 0.01$, Rayleigh Fading).

on MIMO channels. Additionally, an RF energy source can be based on MIMO, e.g. cellular base stations. The energy harvesting can benefit from the energy of multiple antennas. Moreover, instead of considering the distribution of the wireless nodes, different path-loss models, e.g., as discussed in [74], can be adopted to analyze the self-sustainable communication networks. The new path-loss models could be able to represent the non-uniform distributions of the RF energy sources and access points. However, an indepth analysis to evaluate the advantages and disadvantages of these approaches deserves further study.

V. Conclusion

This paper has presented a novel tractable framework based on the Ginibre point process to model and analyze the performance of self-sustainable communications with RF energy harvesting. We have introduced general models that scale well with different distribution patterns, and in different channel fading environments. Specifically, our study has characterized the expectation of RF energy harvesting rate, the energy outage probability and the transmission outage probability over Nakagami-m fading channels. The accuracy of the derived analytical expressions has been validated through numerical simulations. In particular, we observe that when the density of the ambient RF transmitters is small, a larger repulsion among the ambient RF transmitters is able to yield a better transmission outage performance. However, when the density is large, a stronger attraction among the ambient RF transmission renders a lower transmission outage probability. Moreover, the power-splitting architecture outperforms the time-switching architecture in terms of the transmission outage probability. Our analytical framework can be extended by considering uplink transmission from the RF-powered device to the base station. Additionally, it is also interesting to analyze heterogeneous multi-tier cellular networks, e.g., considering underlaying/overlaid small cells and picocells.

Appendix I

Proof of Lemma 1. By independence,

$$\begin{aligned}
&\mathbb{E}\left[\exp\left(-\sum_{k\in\mathcal{K}} h_k\varphi(\mathbf{x}_k)\right)\right]\\
&=\mathbb{E}\left[\mathbb{E}\left[\prod_{k\in\mathcal{K}}\exp\left(-h_k\varphi(\mathbf{x}_k)\right)\mid\mathcal{K}\right]\right]\\
&=\mathbb{E}\left[\prod_{k\in\mathcal{K}}\mathbb{E}\left[\exp\left(-h_k\varphi(\mathbf{x}_k)\right)\right]\right]\\
&=\mathbb{E}\left[\prod_{k\in\mathcal{K}} M_h(-\varphi(\mathbf{x}_k))\right]\\
&=\mathbb{E}\left[\exp\left(-\sum_{k\in\mathcal{K}}-\ln\left(M_h(-\varphi(\mathbf{x}_k))\right)\right)\right].
\end{aligned}$$

By (14),

$$\mathbb{E}\left[\exp\left(-\sum_{k\in\mathcal{K}}-\ln\left(M_h(-\varphi(\mathbf{x}_k))\right)\right)\right]=\mathrm{Det}\left(\mathrm{Id}+\alpha A\right)^{-1/\alpha},$$

where the kernel of A is precisely (20). □

Appendix II

Proof of Lemma 1. Let us begin by recalling that in (3) was proven that $\mathbb{E}\left[\overline{F}/(1+F)\right]=1$. Thus by independence,

$$\begin{aligned}
\mathbb{E}\left[P_{\mathrm{H}}^{TS}\right]&=\tau\beta\left(\mathbb{E}\left[P_{\mathrm{S}}\sum_{k\in\mathcal{K}}\frac{h_k}{(\|\mathbf{x}_k\|+\epsilon)^{\gamma}}\right]+\mathbb{E}\left[\frac{P_{\mathrm{A}}h_{\mathrm{A}}}{\|x_{\mathrm{A}}\|^{\gamma_{\mathrm{A}}}}\right]\right),\\
&=\tau\beta\left(P_{\mathrm{S}}\,\mathbb{E}\left[\sum_{k\in\mathcal{K}}\frac{\mathbb{E}\left[h_k\mid\mathcal{K}\right]}{(\|\mathbf{x}_k\|+\epsilon)^{\gamma}}\right]+\frac{P_{\mathrm{A}}}{\theta_{\mathrm{A}}\|x_{\mathrm{A}}\|^{\gamma_{\mathrm{A}}}}\right),\\
&=\tau\beta\left(\frac{P_{\mathrm{S}}\delta}{\theta}\,\mathbb{E}\left[\sum_{k\in\mathcal{K}}\frac{1}{(\|\mathbf{x}_k\|+\epsilon)^{\gamma}}\right]+\frac{P_{\mathrm{A}}}{\theta_{\mathrm{A}}\|x_{\mathrm{A}}\|^{\gamma_{\mathrm{A}}}}\right).
\end{aligned}$$

Additionally,

$$\mathbb{E}\left[\sum_{k\in\mathcal{K}}\frac{1}{(\|\mathbf{x}_k\|+\epsilon)^{\gamma}}\right]=\int_{\mathcal{B}(0,R)}\frac{\zeta^{(1)}(\mathbf{x})}{(\|\mathbf{x}\|+\epsilon)^{\gamma}}\,\mathrm{d}\mathbf{x},$$

by Campbell's formula [55], where $\zeta^{(1)}(\mathbf{x}) = K(\mathbf{x},\mathbf{x}) = \zeta$ is the intensity function of $\mathcal{K}$ given by (16). Hence,

$$\mathbb{E}[P_{\mathrm{H}}^{TS}] = \tau\beta\left(\frac{P_{\mathrm{S}}\delta}{\theta}\left(2\pi\int_0^R \zeta\frac{r}{(r+\epsilon)^{\gamma}}\,\mathrm{d}r\right) + \frac{P_{\mathrm{A}}}{\theta_{\mathrm{A}}\|x_{\mathrm{A}}\|^{\gamma_{\mathrm{A}}}}\right),$$
$$= \tau\beta\left(\frac{2\pi\zeta P_{\mathrm{S}}\delta}{\theta}\int_0^R \frac{r}{(r+\epsilon)^{\gamma}}\,\mathrm{d}r + \frac{P_{\mathrm{A}}}{\theta_{\mathrm{A}}\|x_{\mathrm{A}}\|^{\gamma_{\mathrm{A}}}}\right),$$

by polar change of variable.

We conclude by computing the latter integral. Let us begin by writing

$$\int_0^R \frac{r}{(r+\epsilon)^{\gamma}}\,\mathrm{d}r = \int_{\epsilon}^{\epsilon+R} u^{1-\gamma}\,\mathrm{d}u - \epsilon\int_{\epsilon}^{\epsilon+R} u^{-\gamma}\,\mathrm{d}u,$$

by change of variable. Thus if $\gamma \neq 1$ and $\gamma \neq 2$,

$$\int_0^R \frac{r}{(r+\epsilon)^{\gamma}}\,\mathrm{d}r = \frac{1}{2-\gamma}\left((\epsilon+R)^{2-\gamma} - \epsilon^{2-\gamma}\right) - \epsilon\frac{1}{1-\gamma}\left((\epsilon+R)^{1-\gamma} - \epsilon^{1-\gamma}\right)$$
$$= \frac{\left(\epsilon^{2-\gamma} - (R+\epsilon)^{1-\gamma}(\epsilon+(\gamma-1)R)\right)}{(\gamma-2)(\gamma-1)}.$$

Similarly,

$$\int_0^R \frac{r}{r+\epsilon}\,\mathrm{d}r = R - \epsilon\left(\ln(\epsilon+R) - \ln(\epsilon)\right),$$

and

$$\int_0^R \frac{r}{(r+\epsilon)^2}\,\mathrm{d}r = \ln(\epsilon+R) - \ln(\epsilon) - \epsilon\left(\frac{1}{\epsilon} - \frac{1}{\epsilon+R}\right),$$

which concludes the proof. □

Appendix III

Proof of Theorem 2. First, notice that (35), where we have used that since $h_{\mathrm{A}} \sim \mathrm{Exp}(\theta_{\mathrm{A}})$,

$$\mathbb{E}\left[\mathrm{e}^{th_{\mathrm{A}}}\right] = \left(1 - \frac{t}{\theta_{\mathrm{A}}}\right)^{-1}, \quad t < 1/\theta_{\mathrm{A}}.$$

Additionally by Lemma 1,

$$\mathbb{E}\left[\exp\left(-\sum_{k\in\mathcal{K}}\frac{\mu\tau\beta\overline{F}P_{\mathrm{S}}h_k}{P_{\mathrm{C}}(\|\mathbf{x}_k\|+\epsilon)^{\gamma}}\right)\right] = \mathrm{Det}\left(\mathrm{Id} + \alpha A\right)^{-1/\alpha},$$

where the kernel of A is precisely (24). Lastly, we note that the only inequality in the previous computation is in (34). Denoting by $X := \frac{\tau\beta\overline{F}}{P_{\mathrm{C}}}\left[\sum_{k\in\mathcal{K}}\frac{P_{\mathrm{S}}h_k}{(\|\mathbf{x}_k\|+\epsilon)^{\gamma}} + \frac{h_{\mathrm{A}}P_{\mathrm{A}}}{\|\mathbf{x}_{\mathrm{A}}\|^{\gamma_{\mathrm{A}}}}\right]$, one has

$$0 \leq \mathbb{P}\left(P_{\mathrm{H}}^{TS} < P_{\mathrm{C}}\right) - \left(1 + \frac{\mu\tau\beta\overline{F}P_{\mathrm{A}}}{\theta_{\mathrm{A}}P_{\mathrm{C}}\|\mathbf{x}_{\mathrm{A}}\|^{\gamma_{\mathrm{A}}}}\right)^{-1}\mathrm{Det}\left(\mathrm{Id}+\alpha A\right)^{-1/\alpha}$$
$$= \mathbb{P}\left(F > \frac{\tau\beta\overline{F}}{P_{\mathrm{C}}}\left[\sum_{k\in\mathcal{K}}\frac{P_{\mathrm{S}}h_k}{(\|\mathbf{x}_k\|+\epsilon)^{\gamma}} + \frac{h_{\mathrm{A}}P_{\mathrm{A}}}{\|\mathbf{x}_{\mathrm{A}}\|^{\gamma_{\mathrm{A}}}}\right] - 1\right)$$
$$- \mathbb{P}\left(F > \frac{\tau\beta\overline{F}}{P_{\mathrm{C}}}\left[\sum_{k\in\mathcal{K}}\frac{P_{\mathrm{S}}h_k}{(\|\mathbf{x}_k\|+\epsilon)^{\gamma}} + \frac{h_{\mathrm{A}}P_{\mathrm{A}}}{\|\mathbf{x}_{\mathrm{A}}\|^{\gamma_{\mathrm{A}}}}\right]\right)$$
$$= \mathbb{P}\left(F > X - 1\right) - \mathbb{P}\left(F > X\right)$$
$$= \mathbb{E}\left[\left(\mathrm{e}^{-\mu(X-1)} - \mathrm{e}^{-\mu X}\right)1_{\{X\geq 1\}} + \left(1 - \mathrm{e}^{-\mu X}\right)1_{\{X<1\}}\right]$$
$$\leq \mathbb{E}\left[\left(1 - \mathrm{e}^{-\mu}\right)1_{\{X\geq 1\}} + \left(1 - \mathrm{e}^{-\mu}\right)1_{\{X<1\}}\right]$$
$$= 1 - \mathrm{e}^{-\mu},$$

which concludes the proof. □

Appendix IV

Proof of Theorem 3. Let g_{A} be a random variable with the same law as h_{A} and independent from the rest. Define $\hat{C}^{TS}$ as in (4):

$$\hat{C}^{TS} = \begin{cases}(1-\tau)W\log_2\left(1 + \frac{g_{\mathrm{A}}P_{\mathrm{A}}/\|\mathbf{x}_{\mathrm{A}}\|^{\gamma_{\mathrm{A}}}}{\sigma^2+\xi I^{TS}}\right) & \text{if } P_{\mathrm{H}}^{TS} \geq P_{\mathrm{C}},\\ 0 & \text{if } P_{\mathrm{H}}^{TS} < P_{\mathrm{C}},\end{cases}$$

with g_{A} in place of h_{A}. We base the rest of the proof on the approximation $\mathbb{P}\left(C^{TS} < \kappa\right) \simeq \mathbb{P}(\hat{C}^{TS} < \kappa)$. Since $g_{\mathrm{A}}, h_{\mathrm{A}} \sim \mathrm{Exp}(\theta_{\mathrm{A}})$, by (19), we have (36). and by the same approximation as in Theorem 2 we obtain by conditioning (37).

Now recall that since $h_1 \sim \Gamma(\delta,\theta)$,

$$\mathbb{E}\left[\mathrm{e}^{th_1}\right] = \left(1 - \frac{t}{\theta}\right)^{-\delta}, \quad t < 1/\theta,$$

hence by Lemma 1, we conclude (38) and (39), respectively.

The result follows immediately by the approximation $\mathbb{P}\left(C^{TS} < \kappa\right) \simeq \mathbb{P}(\hat{C}^{TS} < \kappa)$. □

Acknowledgment

This work was supported in part by the Singapore MOE Tier 1 (RG18/13 and RG33/12) and MOE Tier 2 (MOE2012-T2-2-033 ARC 3/13 and MOE2014-T2-2-015 ARC 4/15), and National Research Foundation of Korea (NRF) grant funded by the Korean government (MSIP) (2014R1A5A1011478).

References

[1] S. Ulukus, A. Yener, E. Erkip, O. Simeone, M. Zorzi, P. Grover and K. Huang, "Energy Harvesting Wireless Communications: A Review of Recent Advances," *IEEE Journal of Selected Areas in Communications*, vol. 33, no. 3, pp. 360-381, Mar. 2015.

[2] D. Niyato, X. Lu, P. Wang, D. I. Kim, and Z. Han, "Economics of Internet of Things (IoT): An Information Market Approach," to appear in *IEEE Wireless Communications*.

[3] D. Niyato, X. Lu, and P. Wang, "Machine-to-Machine Communications for Home Energy Management System in Smart Grid," IEEE Communications, vol. 49, no. 4, pp. 53-59, April 2011.

[4] X. Lu "Sensor Networks with Wireless Energy Harvesting," in *Wireless-Powered Communication Networks: Architecture, Protocols and Applications*, (Eds. D. Niyato, E. Hossian, D. I. Kim, V. Bhargava, L. Shafai), Cambridge University Press, 2016.

[5] I. Krikidis, S. Timotheou, S. Nikolaou, G. Zheng, D. W. K. Ng, and R. Schober, "Simultaneous Wireless Information and Power Transfer in Modern Communication systems," *IEEE Communications Magazine*, vol. 52, no. 11, Nov. 2014.

[6] K. Huang and E. G. Larsson, "Simultaneous Information and Power Transfer for Broadband Wireless Systems," *IEEE Trans. on Signal Processing*, vol. 61, no. 23, pp. 5972-5986, Dec. 2013.

[7] X. Lu, I. Flint, D. Niyato, N. Privault, and P. Wang, "Performance Analysis for Simultaneously Wireless Information and Power Transfer with Ambient RF Energy Harvesting," in *Proc. of IEEE WCNC*, New Orleans, LA, USA, March 2015.

[8] X. Lu, P. Wang, D. Niyato, and Z. Han, "Resource Allocation in Wireless Networks with RF Energy Harvesting and Transfer," *IEEE Network*, vol. 29, no. 6, pp. 68-75, Dec. 2015.

[9] X. Lu, P. Wang, D. Niyato, D. I. Kim, and Z. Han, "Wireless Charger Networking for Mobile Devices: Fundamentals, Standards, and Applications," *IEEE Wireless Communications*, vol. 22, no. 2, pp. 126-135, April 2015.

[10] X. Lu, P. Wang, D. Niyato, and E. Hossain, "Dynamic Spectrum Access in Cognitive Radio Networks with RF Energy Harvesting," *IEEE Wireless Communications*, vol. 21, no. 3, pp. 102-110, June 2014.

$$\mathbb{P}\left(P_{\mathrm{H}}^{TS}<P_{\mathrm{C}}\right)=\mathbb{P}\left(\frac{\tau\beta\overline{F}}{1+F}\left[\sum_{k\in\mathcal{K}}\frac{P_{\mathrm{S}}h_k}{(\|\mathbf{x}_k\|+\epsilon)^{\gamma}}+\frac{h_{\mathrm{A}}P_{\mathrm{A}}}{\|\mathbf{x}_{\mathrm{A}}\|^{\gamma_{\mathrm{A}}}}\right]<P_{\mathrm{C}}\right)=\mathbb{P}\left(\frac{\tau\beta\overline{F}}{P_{\mathrm{C}}}\left[\sum_{k\in\mathcal{K}}\frac{P_{\mathrm{S}}h_k}{(\|\mathbf{x}_k\|+\epsilon)^{\gamma}}+\frac{h_{\mathrm{A}}P_{\mathrm{A}}}{\|\mathbf{x}_{\mathrm{A}}\|^{\gamma_{\mathrm{A}}}}\right]-1<F\right)$$
$$\geq\mathbb{P}\left(\frac{\tau\beta\overline{F}}{P_{\mathrm{C}}}\left[\sum_{k\in\mathcal{K}}\frac{P_{\mathrm{S}}h_k}{(\|\mathbf{x}_k\|+\epsilon)^{\gamma}}+\frac{h_{\mathrm{A}}P_{\mathrm{A}}}{\|\mathbf{x}_{\mathrm{A}}\|^{\gamma_{\mathrm{A}}}}\right]<F\right) \tag{34}$$
$$=\mathbb{E}\left[\exp\left(-\frac{\mu\tau\beta\overline{F}}{P_{\mathrm{C}}}\left[\sum_{k\in\mathcal{K}}\frac{P_{\mathrm{S}}h_k}{(\|\mathbf{x}_k\|+\epsilon)^{\gamma}}+\frac{h_{\mathrm{A}}P_{\mathrm{A}}}{\|\mathbf{x}_{\mathrm{A}}\|^{\gamma_{\mathrm{A}}}}\right]\right)\right]=\mathbb{E}\left[\exp\left(-\sum_{k\in\mathcal{K}}\frac{\mu\tau\beta\overline{F}P_{\mathrm{S}}h_k}{P_{\mathrm{C}}(\|\mathbf{x}_k\|+\epsilon)^{\gamma}}\right)\right]\cdot\mathbb{E}\left[\exp\left(-\frac{\mu\tau\beta P_{\mathrm{A}}\overline{F}}{P_{\mathrm{C}}\|\mathbf{x}_{\mathrm{A}}\|^{\gamma_{\mathrm{A}}}}h_{\mathrm{A}}\right)\right]$$
$$=\left(1+\frac{\mu\tau\beta P_{\mathrm{A}}\overline{F}}{\theta_{\mathrm{A}}P_{\mathrm{C}}\|\mathbf{x}_{\mathrm{A}}\|^{\gamma_{\mathrm{A}}}}\right)^{-1}\mathbb{E}\left[\exp\left(-\sum_{k\in\mathcal{K}}\frac{\mu\tau\beta\overline{F}P_{\mathrm{S}}h_k}{P_{\mathrm{C}}(\|\mathbf{x}_k\|+\epsilon)^{\gamma}}\right)\right], \tag{35}$$

$$\mathbb{P}\left(\hat{C}^{TS}<\kappa\right)$$
$$=\mathbb{P}\left(P_{\mathrm{H}}^{TS}<P_{\mathrm{C}}\right)+\mathbb{P}\left(1+\frac{g_{\mathrm{A}}P_{\mathrm{A}}}{\|\mathbf{x}_{\mathrm{A}}\|^{\gamma_{\mathrm{A}}}\left(\sigma^2+\xi\sum_{k\in\mathcal{K}}P_{\mathrm{S}}h_k/(\|\mathbf{x}_k\|+\epsilon)^{\gamma}\right)}<2^{\kappa/(W(1-\tau))},\ P_{\mathrm{H}}^{TS}\geq P_{\mathrm{C}}\right)$$
$$=\mathbb{P}\left(P_{\mathrm{H}}^{TS}<P_{\mathrm{C}}\right)+\mathbb{P}\left(g_{\mathrm{A}}<\frac{\|\mathbf{x}_{\mathrm{A}}\|^{\gamma_{\mathrm{A}}}}{P_{\mathrm{A}}}\left(2^{\kappa/(W(1-\tau))}-1\right)\left(\sigma^2+\xi\sum_{k\in\mathcal{K}}\frac{P_{\mathrm{S}}h_k}{(\|\mathbf{x}_k\|+\epsilon)^{\gamma}}\right),\ P_{\mathrm{H}}^{TS}\geq P_{\mathrm{C}}\right)$$
$$=\mathbb{P}\left(P_{\mathrm{H}}^{TS}<P_{\mathrm{C}}\right)+\mathbb{E}\left[\left(1-\exp\left(-\frac{\theta_{\mathrm{A}}\|\mathbf{x}_{\mathrm{A}}\|^{\gamma_{\mathrm{A}}}}{P_{\mathrm{A}}}\left(2^{\kappa/(W(1-\tau))}-1\right)\left(\sigma^2+\xi\sum_{k\in\mathcal{K}}\frac{P_{\mathrm{S}}h_k}{(\|\mathbf{x}_k\|+\epsilon)^{\gamma}}\right)\right)\right)1_{\{P_{\mathrm{H}}^{TS}\geq P_{\mathrm{C}}\}}\right]$$
$$=1-\exp\left(-\frac{\theta_{\mathrm{A}}\sigma^2\|\mathbf{x}_{\mathrm{A}}\|^{\gamma_{\mathrm{A}}}}{P_{\mathrm{A}}}\left(2^{\kappa/(W(1-\tau))}-1\right)\right)\mathbb{E}\left[\exp\left(-\frac{\theta_{\mathrm{A}}\|\mathbf{x}_{\mathrm{A}}\|^{\gamma_{\mathrm{A}}}}{P_{\mathrm{A}}}\left(2^{\kappa/(W(1-\tau))}-1\right)\xi\sum_{k\in\mathcal{K}}\frac{P_{\mathrm{S}}h_k}{(\|\mathbf{x}_k\|+\epsilon)^{\gamma}}\right)1_{\{P_{\mathrm{H}}^{TS}\geq P_{\mathrm{C}}\}}\right]$$
$$=1-\exp\left(-\frac{\theta_{\mathrm{A}}\sigma^2\|\mathbf{x}_{\mathrm{A}}\|^{\gamma_{\mathrm{A}}}}{P_{\mathrm{A}}}\left(2^{\kappa/(W(1-\tau))}-1\right)\right)$$
$$\times\mathbb{E}\left[\exp\left(-\frac{\theta_{\mathrm{A}}\|\mathbf{x}_{\mathrm{A}}\|^{\gamma_{\mathrm{A}}}}{P_{\mathrm{A}}}\left(2^{\kappa/(W(1-\tau))}-1\right)\xi\sum_{k\in\mathcal{K}}\frac{P_{\mathrm{S}}h_k}{(\|\mathbf{x}_k\|+\epsilon)^{\gamma}}\right)1_{\left\{\frac{\tau\beta\overline{F}}{P_{\mathrm{C}}}\left[\sum_{k\in\mathcal{K}}\frac{P_{\mathrm{S}}h_k}{(\|\mathbf{x}_k\|+\epsilon)^{\gamma}}+\frac{h_{\mathrm{A}}P_{\mathrm{A}}}{\|\mathbf{x}_{\mathrm{A}}\|^{\gamma_{\mathrm{A}}}}\right]-1\geq F\right\}}\right], \tag{36}$$

$$\mathbb{P}\left(\hat{C}^{TS}<\kappa\right)$$
$$\simeq\ 1-\exp\left(-\frac{\theta_{\mathrm{A}}\sigma^2\|\mathbf{x}_{\mathrm{A}}\|^{\gamma_{\mathrm{A}}}}{P_{\mathrm{A}}}\left(2^{\kappa/(W(1-\tau))}-1\right)\right)\mathbb{E}\left[\exp\left(-\frac{\theta_{\mathrm{A}}\|\mathbf{x}_{\mathrm{A}}\|^{\gamma_{\mathrm{A}}}}{P_{\mathrm{A}}}\left(2^{\kappa/(W(1-\tau))}-1\right)\xi\sum_{k\in\mathcal{K}}\frac{P_{\mathrm{S}}h_k}{(\|\mathbf{x}_k\|+\epsilon)^{\gamma}}\right)\right.$$
$$\left.\times\left(1-\exp\left(-\frac{\mu\tau\beta\overline{F}}{P_{\mathrm{C}}}\left[\sum_{k\in\mathcal{K}}\frac{P_{\mathrm{S}}h_k}{(\|\mathbf{x}_k\|+\epsilon)^{\gamma}}+\frac{h_{\mathrm{A}}P_{\mathrm{A}}}{\|\mathbf{x}_{\mathrm{A}}\|^{\gamma_{\mathrm{A}}}}\right]\right)\right)\right]$$
$$=\ 1-\exp\left(-\frac{\theta_{\mathrm{A}}\sigma^2\|\mathbf{x}_{\mathrm{A}}\|^{\gamma_{\mathrm{A}}}}{P_{\mathrm{A}}}\left(2^{\kappa/(W(1-\tau))}-1\right)\right)\left(\mathbb{E}\left[\exp\left(-\frac{\theta_{\mathrm{A}}\|\mathbf{x}_{\mathrm{A}}\|^{\gamma_{\mathrm{A}}}}{P_{\mathrm{A}}}\left(2^{\kappa/(W(1-\tau))}-1\right)\xi\sum_{k\in\mathcal{K}}\frac{P_{\mathrm{S}}h_k}{(\|\mathbf{x}_k\|+\epsilon)^{\gamma}}\right)\right]\right.$$
$$\left.-\left(1+\frac{\mu\tau\beta P_{\mathrm{A}}\overline{F}}{P_{\mathrm{C}}\|\mathbf{x}_{\mathrm{A}}\|^{\gamma_{\mathrm{A}}}\theta_{\mathrm{A}}}\right)^{-1}\mathbb{E}\left[\exp\left(-\left(\frac{\mu\tau\beta\overline{F}}{P_{\mathrm{C}}}+\frac{\theta_{\mathrm{A}}\|\mathbf{x}_{\mathrm{A}}\|^{\gamma_{\mathrm{A}}}}{P_{\mathrm{A}}}\left(2^{\kappa/(W(1-\tau))}-1\right)\xi\right)\sum_{k\in\mathcal{K}}\frac{P_{\mathrm{S}}h_k}{(\|\mathbf{x}_k\|+\epsilon)^{\gamma}}\right)\right]\right) \tag{37}$$

$$\mathbb{E}\left[\exp\left(-\frac{\theta_{\mathrm{A}}\|\mathbf{x}_{\mathrm{A}}\|^{\gamma_{\mathrm{A}}}}{P_{\mathrm{A}}}\left(2^{\kappa/(W(1-\tau))}-1\right)\xi\sum_{k\in\mathcal{K}}\frac{P_{\mathrm{S}}h_k}{(\|\mathbf{x}_k\|+\epsilon)^{\gamma}}\right)\right]=\mathrm{Det}\left(\mathrm{Id}+\alpha A_m\right)^{-1/\alpha}, \tag{38}$$

$$\mathbb{E}\left[\exp\left(-\left(\frac{\mu\tau\beta\overline{F}P_{\mathrm{A}}+P_{\mathrm{C}}\theta_{\mathrm{A}}\|\mathbf{x}_{\mathrm{A}}\|^{\gamma_{\mathrm{A}}}\left(2^{\kappa/(W(1-\tau))}-1\right)\xi}{P_{\mathrm{C}}P_{\mathrm{A}}}\right)\sum_{k\in\mathcal{K}}\frac{P_{\mathrm{S}}h_k}{(\|\mathbf{x}_k\|+\epsilon)^{\gamma}}\right)\right]=\mathrm{Det}\left(\mathrm{Id}+\alpha B_m\right)^{-1/\alpha}. \quad (39)$$

[11] C. Liu, M. Maso, S. Lakshminarayana, C. Lee, and T. Q. S. Quek, "Simultaneous Wireless Information and Power Transfer Under Different CSI Acquisition Schemes," *IEEE Transactions on Wireless Communications*, vol. 14, no. 4, pp. 1911-1926, April 2015.

[12] S. Timotheou, I. Krikidis, S. Karachontzitis, and K. Berberidis, "Spatial Domain Simultaneous Information and Power Transfer for MIMO Channels," *IEEE Transactions on Wireless Communications*, vol. 14, no. 8, pp. 4115-4128, Aug. 2015.

[13] A. A. Nasir, X. Zhou, S. Durrani, and R. A. Kennedy, "Relaying Protocols for Wireless Energy Harvesting and Information Processing," *IEEE Transactions on Wireless Communications*, vol. 12, no. 7, pp. 3622-3636, July 2013.

[14] X. Chen, Z. Zhang, H. Chen, and H. Zhang, "Enhancing wireless information and power transfer by exploiting multi-antenna techniques," *IEEE Communications Magazine*, vol. 53, no. 4, pp. 133-141, April 2015.

[15] D. W. K. Ng, E. S. Lo, and R. Schober, "Robust Beamforming for Secure Communication in Systems With Wireless Information and Power Transfer," *IEEE Transactions on Wireless Communications*, vol. 13, no. 8, pp. 4599-4615, Aug. 2014.

[16] D. W. K. Ng, E. S. Lo, and R. Schober, "Wireless Information and Power Transfer: Energy Efficiency Optimization in OFDMA Systems," *IEEE Transactions on Wireless Communications*, vol. 12, no. 12, pp. 6352-6370, December 2013.

[17] D. W. K. Ng, E. S. Lo, and R. Schober, "Multi-Objective Resource Allocation for Secure Communication in Cognitive Radio Networks with Wireless Information and Power Transfer," to appear in *IEEE Transactions on Vehicular Technology*.

[18] D. W. K. Ng, and R. Schober, "Secure and Green SWIPT in Distributed Antenna Networks with Limited Backhaul Capacity," *IEEE Transaction on Wireless Communications*, vol. 14, no. 9, pp. 5082-5097, Sept. 2015.

[19] D. W. K. Ng, and R. Schober, "Secure and Green SWIPT in Distributed Antenna Networks with Limited Backhaul Capacity," *IEEE Transactions on Wireless Communications*, vol. 14, no. 9, no. 5082-5097, Sept. 2015.

[20] Y. Zeng, and R. Zhang, "Full-Duplex Wireless-Powered Relay With Self-Energy Recycling," *IEEE Wireless Communications Letters*, vol. 4, no. 2, pp. 201-204, April 2015.

[21] Z. Wen, X. Liu, N. C. Beaulieu, R. Wang, and S. Wang, "Joint Source and Relay Beamforming Design for Full-Duplex MIMO AF Relay SWIPT Systems," *IEEE Communications Letters*, vol. 20, no. 2, pp. 320-323, Feb. 2016.

[22] S. Kim, R. Vyas, J. Bito, K. Niotaki, A. Collado, A. Georgiadis, and M. M. Tentzeris, "Ambient RF Energy-Harvesting Technologies for Self-Sustainable Standalone Wireless Sensor Platforms," *Proceedings of the IEEE*, vol. 102, no. 11, pp. 1649-1666, Nov. 2014.

[23] H. Sun, Y. Guo, M. He, and Z. Zhong, "A Dual-Band Rectenna Using Broadband Yagi Antenna Array for Ambient RF Power Harvesting," *IEEE Antennas and Wireless Propagation Letters*, vol. 12, pp. 918-921, August 2013.

[24] G. A. Vera, D. Allane, A. Georgiadis, A. Collado, Y. Duroc, and S. Tedjini, "Cooperative Integration of Harvesting RF Sections for Passive RFID Communication," vol. 63, no. 12, pp. 4556-4566, *IEEE Transactions on Microwave Theory and Techniques*, Dec. 2015.

[25] M. Fantuzzi, D. Masotti, and A. Costanzo, "Simultaneous UHF energy harvesting and UWB-RFID communication," in Proc. of *IEEE MTT-S International Microwave Symposium (IMS)*, Phoenix, AZ, May 2015.

[26] F. Goodarzy, E. Skafidas, and S. Gambini, "Feasibility of Energy-Autonomous Wireless Microsensors for Biomedical Applications: Powering and Communication," *IEEE Reviews in Biomedical Engineering*, vol. 8, pp. 17-29, Aug. 2015.

[27] D. Niyato, X. Lu, P. Wang, D. I. Kim and Z. Han, "Distributed Wireless Energy Scheduling for Wireless Powered Sensor Networks," in *Proc. of IEEE ICC*, Kuala Lumpur, Malaysia, 23-27, May 2016.

[28] C. Boyer, and S. Roy, "Backscatter Communication and RFID: Coding, Energy, and MIMO Analysis," *IEEE Transactions on Communications*, 2014 vol. 62, no. 3, pp. 770-785, March 2014.

[29] R. Correia, N. B. de Carvalho, G. Fukuday, A. Miyaji, and S. Kawasaki, "Backscatter wireless sensor network with WPT capabilities," in Proc. of *IEEE MTT-S International Microwave Symposium (IMS)*, Phoenix, AZ, May 2015.

[30] S. H. Choi, and D. I. Kim, "Backscatter radio communication for wireless powered communication networks," in *Proc. of IEEE Asia-Pacific Conference on Communications (APCC)*, Kyoto, Japan, Oct. 2015.

[31] N. Jose, N. John, P. Jain, P. Raja, T.V. Prabhakar, and K. J. Vinoy, "RF powered integrated system for IoT applications," in Proc. of *IEEE 13th International New Circuits and Systems Conference (NEWCAS)*, Grenoble, France, June 2015.

[32] M. M. Tentzeris, A. Georgiadis, and L. Roselli, "Energy Harvesting and Scavenging," *Proceedings of the IEEE*, vol. 102, no. 11 pp. 1644-1648, Nov. 2014.

[33] X. Lu, P. Wang, D. Niyato, D. I. Kim, and Z. Han, "Wireless Charging Technologies: Fundamentals, Standards, and Network Applications," to appear in *IEEE Communications Surveys and Tutorials*.

[34] X. Lu, P. Wang, D. Niyato, D. I. Kim, and H, Zhu, "Wireless Networks with RF Energy Harvesting: A Contemporary Survey," *IEEE Communications Surveys and Tutorials*, vol. 17, no. 2, pp. 757-789, May 2015.

[35] K. Huang, and V. K. N. Lau, "Enabling Wireless Power Transfer in Cellular Networks: Architecture, Modeling and Deployment," *IEEE Transactions on Wireless Communications*, vol. 13, no. 2, pp. 902-912, Feb. 2014.

[36] A. H. Sakr and E. Hossain, "Analysis of K-tier Uplink Cellular Networks with Ambient RF Energy Harvesting," *IEEE Journal on Selected Areas in Communications*, vol. 33, no. 10, pp. 2226-2238, Oct. 2015.

[37] I. Krikidis, "Simultaneous Information and Energy Transfer in Large-Scale Networks with/without Relaying," *IEEE Transactions on Communications*, vol. 62, no. 3, pp. 900-912, March 2014.

[38] P.-V. Mekikis, A. S. Lalos, A. Antonopoulos, L. Alonso, and C. Verikoukis, "Wireless Energy Harvesting in Two-Way Network Coded Cooperative Communications: A Stochastic Approach for Large Scale Networks," *IEEE Communications Letters*, vol. 18, no. 6, pp. 1011-1014, June 2014.

[39] Z. Ding, I. Krikidis, B. Sharif, and H. V. Poor, "Wireless Information and Power Transfer in Cooperative Networks With Spatially Random Relays," *IEEE Transactions on Wireless Communications*, vol. 13, no. 8, pp. 4440-4453, Aug. 2014.

[40] S. Lee, R. Zhang, and K. Huang, "Opportunistic Wireless Energy Harvesting in Cognitive Radio Networks," *IEEE Transactions on Wireless Communications*, vol. 12, no. 9, pp. 4788-4799, Sept. 2013.

[41] A. H. Sakr and E. Hossain, "Cognitive and Energy Harvesting-Based D2D Communication in Cellular Networks: Stochastic Geometry Modeling and Analysis," *IEEE Transactions on Communications*, vol. 63, no. 5, pp. 1867-1880, May 2015.

[42] Y. L. Che, L. Duan and R. Zhang, "Spatial Throughput Maximization of Wireless Powered Communication Networks," *IEEE Journal on Selected Areas in Communications*, vol. 33, no. 8, pp. 1534-1548, Aug. 2015.

[43] J. G. Andrews, F. Baccelli, and R.K. Ganti, "A Tractable Approach to Coverage and Rate in Cellular Networks," in *Communications, IEEE Transactions on*, vol. 59, pp. 3122-3134, Nov. 2011.

[44] T.-Y. Lin, H. Santoso, and K.-R. Wu, "Global Sensor Deployment and Local Coverage-Aware Recovery Schemes for Smart Environments," *IEEE Trans. Mobile Comput.*, vol. 14, pp. 13821396, Jul. 2015.

[45] S. Cho, and W. Choi, "Energy-efficient Repulsive Cell Activation for Heterogeneous Cellular Networks," *IEEE Journal on Selected Areas in Communications*, vol. 31, no. 5, pp. 870-882, May 2013.

[46] M. Kountouris, and N. Pappas, "Approximating the Interference Distribution in Large Wireless Networks," in *Proc. of International Symposium on Wireless Communications Systems (ISWCS)*, Barcelona, Spain, Aug. 2014.

[47] L. Decreusefond, I. Flint, and A. Vergne, "Efficient Simulation of the Ginibre Point Process." *Advances in applied probability*, vol. 52, no. 4, Oct. 2015.

[48] N. Deng, W. Zhou, and M. Haenggi, "The Ginibre Point Process as a Model for Wireless Networks with Repulsion," *Transactions on Wireless Communications*, vol. 14, no. 1, pp. 107 - 121, Jan. 2015.

[49] I. Flint, X. Lu, N. Privault, D. Niyato, and P. Wang, "Performance Analysis of Ambient RF Energy Harvesting with Repulsive Point

Process Modeling," *IEEE Transactions on Wireless Communications*, vol. 14, no. 10, pp. 5402-5416, May 2015.

[50] I. Nakata, and N. Miyoshi, "Spatial Stochastic Models for Analysis of Heterogeneous Cellular Networks with Repulsively Deployed Base Stations," *Performance Evaluation*, vol. 78, pp. 7-17, Aug. 2014.

[51] J. Gomez, A. Vasseur, A. Vergne, P. Martins, L. Decreusefond, and W. Chen, "A Case Study on Regularity in Cellular Network Deployment," *IEEE Wireless Communications Letters*, vol. 4, no. 4, pp. 421 - 424, Aug. 2015.

[52] T. Kobayashi, and N. Miyoshi, "Uplink Cellular Network Models with Ginibre Deployed Base Stations," in *Proc. of Teletraffic Congress (ITC)*, Karlskrona, Sweden, Sept. 2014.

[53] I. Flint, X. Lu, N. Privault, D. Niyato, and P. Wang, "Performance Analysis of Ambient RF Energy Harvesting: A Stochastic Geometry Approach," in *Proc. of IEEE Globecom*, Austin, USA, December 2014.

[54] X. Zhou, R. Zhang, and C. K. Ho, "Wireless Information and Power Transfer: Architecture Design and Rate-energy Tradeoff," *IEEE Transactions on Communications*, vol. 61, no. 11, pp. 4757-4767, November, 2013.

[55] O. Kallenberg, *Random measures,* fourth ed. Berlin, Germany: Akademie-Verlag, 1986.

[56] G. Miao, N. Himayat, Y. G. Li, and A. Swami, "Cross-layer Optimization for Energy-efficient Wireless Communications: A Survey," *Wireless Commun. Mobile Comput.*, vol. 9, pp. 529-542, Apr. 2009.

[57] D. J. Daley and D. Vere-Jones, *An Introduction to the Theory of Point Processes. Vol. I,* 2nd ed. New York: Springer-Verlag, Probability and its Applications, 2003.

[58] T. Shirai and Y. Takahashi, "Random Point Fields Associated with Certain Fredholm Determinants I: Fermion, Poisson and Boson Point Processes," *Journal of Functional Analysis*, vol. 205, no. 2, pp. 414-463, December 2003.

[59] H. Brezis, *Analyse fonctionnelle,* Paris, France: Masson, Collection Mathématiques Appliquées pour la Maîtrise. [Collection of Applied Mathematics for the Master's Degree], 1983.

[60] D. Vere-Jones, "A Generalization of Permanents and Determinants," in *Linear Algebra Appl.*, vol. 111, pp. 119-124, 1988.

[61] H. Georgii and H. J. Yoo, "Conditional Intensity and Gibbsianness of Determinantal Point Processes," in *J. Stat. Phys.*, 118(1-2):55-84, 2005.

[62] A. Soshnikov. Determinantal Random Point Fields. *Uspekhi Mat. Nauk*, 55(5(335)):107–160, 2000.

[63] A. Goldman. "The Palm Measure and the Voronoi Tessellation for the Ginibre Process." *Ann. Appl. Probab.*, vol. 20, no. 1, pp. 90–128, 2010.

[64] F. Bornemann. On the Numerical Evaluation of Fredholm Determinants. *Math. Comp.*, 79(270):871–915, 2010.

[65] J. B. Hough, M. Krishnapur, Y. Peres, and B. Virág. Determinantal processes and independence. *Probab. Surv.*, 3:1549-5787, 2006.

[66] L. Decreusefond, I. Flint, N. Privault, and G. L. Torrisi. Determinantal point processes: a survey. to appear in "Stochastic Analysis for Poisson Point Processes: Malliavin Calculus, Wiener-It Chaos Expansions and Stochastic Geometry", edited by G. Peccati and M. Reitzner, Bocconi & Springer Series, Springer, 2016.

[67] L. Decreusefond, I. Flint, N. Privault, and G. L. Torrisi. Stochastic dynamics of determinantal processes by integration by parts, to appear in *Communications on Stochastic Analysis*.

[68] C. Chung, Y. Kim, T. Ki, K. Bae, and J. Kim, "Fully Integrated Ultra-low-power 900 MHz RF Transceiver for Batteryless Wireless Microsystems," in *Proc. of IEEE International Conference on Electronics, Circuits and Systems (ICECS)*, Beirut, Lebanon, Dec. 2011.

[69] L. Liu, R. Zhang, and K. Chua, "Wireless Information and Power Transfer: A Dynamic Power Splitting Approach," *IEEE Transactions on Communications*, vol. 61, no. 9, pp. 3990-4001, Sept. 2013.

[70] X. Zhou, J. Guo, S. Durrani, and I. Krikidis, "Performance of Maximum Ratio Transmission in Ad Hoc Networks with SWIPT," *IEEE Wireless Communications Letters*, vol. 4, no. 5, pp. 529-532, Oct. 2015.

[71] R. Morsi, D. S. Michalopoulos, and R. Schober, "Multiuser Scheduling Schemes for Simultaneous Wireless Information and Power Transfer Over Fading Channels," *IEEE Transactions on Wireless Communications*, vol. 14, no. 4, pp. 1967-1982, Apr. 2015.

[72] M. Cardenas-Juarez and M. Ghogho, "Spectrum Sensing and Throughput Trade-off in Cognitive Radio under Outage Constraints over Nakagami Fading," *IEEE Communications Letters*, vol. 15, no. 10, pp. 1110-1113, Oct. 2011.

[73] Z. Ding, C. Zhong, D. W. K. Ng, M. Peng, H. A. Suraweera, R. Schober and H. V. Poor, "Application of Smart Antenna Technologies in Simultaneous Wireless Information and Power Transfer," *IEEE Communications*, vol. 53, pp. 86-93, April 2015.

[74] K. Ishibashi and G. Abreu, "Analysis of RF Energy Harvesting in Large-scale Networks Using Absorption Function," in *Proceedings of International Conference on Acoustics, Speech and Signal Processing (ICASSP)*, pp. 7004-7008, May 2014.